iScience

CellPress
OPEN ACCESS

Article

The E3 Ubiquitin Ligase SYVN1 Ubiquitinates Atlastins to Remodel the Endoplasmic Reticulum Network

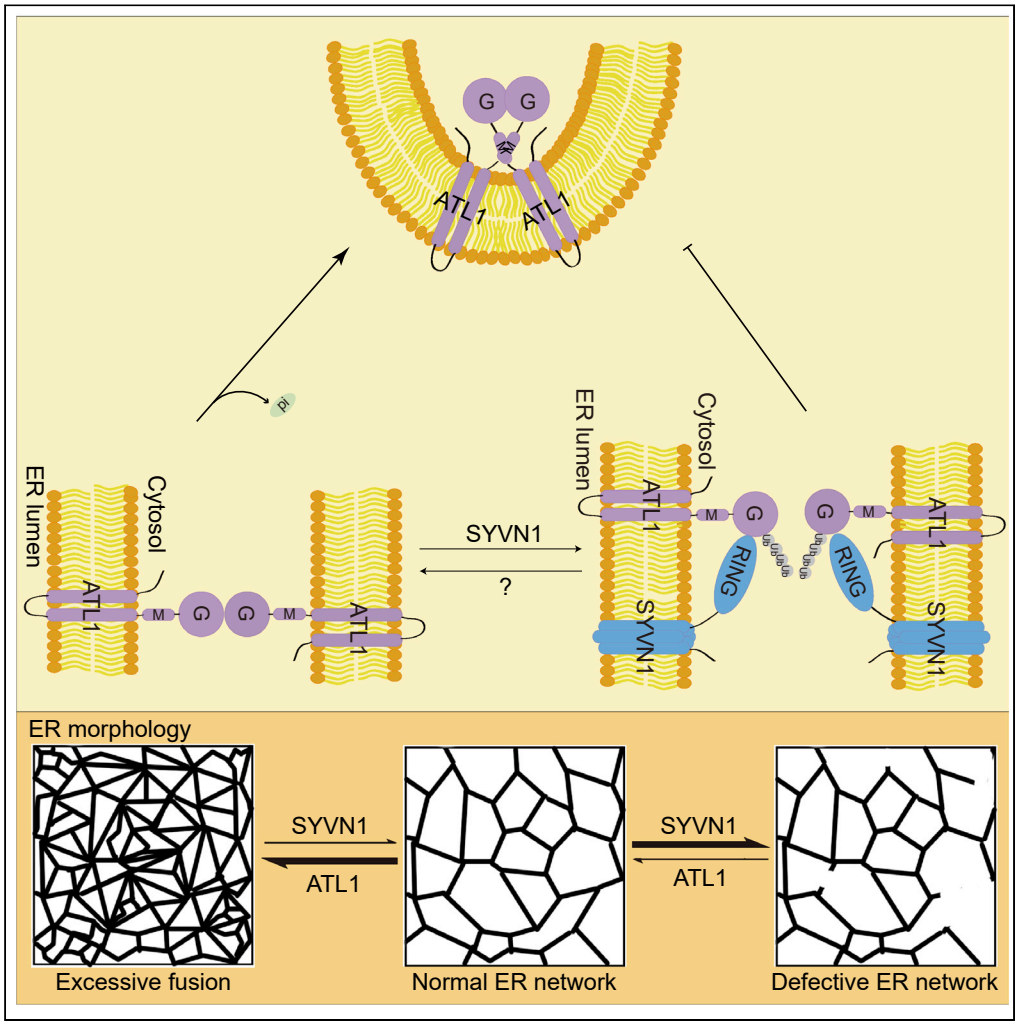

Yupeng Zhao, Zhigang Feng, Yan Zou, Yanfen Liu

zouyan@shanghaitech.edu.cn (Y.Z.)
liuyf@shanghaitech.edu.cn (Y.L.)

HIGHLIGHTS

The E3 ubiquitin ligase SYVN1 ubiquitinates GTPase ATLs to regulate ER membrane fusion

SYVN1 plays an opposite role to ATL1 in ER network remodeling

Ubiquitination on ATL1 by SYVN1 inhibits ATL1 GTPase activity

The role of SYVN1 and ATL1 in ER remodeling is recapitulated *in vivo*

Zhao et al., iScience *23*, 101494
September 25, 2020
https://doi.org/10.1016/j.isci.2020.101494

iScience

CellPress
OPEN ACCESS

Article

The E3 Ubiquitin Ligase SYVN1 Ubiquitinates Atlastins to Remodel the Endoplasmic Reticulum Network

Yupeng Zhao,[1,2,4,5] Zhigang Feng,[1,3,4,5] Yan Zou,[1,3,4,*] and Yanfen Liu[1,2,4,6,*]

SUMMARY

Atlastin (ATL) is a class of dynamin-like GTPases shaping endoplasmic reticulum (ER) by mediating homotypic membrane fusion. Defect of ATLs leads to abnormal ER structure and hereditary spastic paraplegia (HSP), a neurodegenerative disease with progressive spasticity. How ATLs are regulated to maintain the ER dynamics is not clear. Here, we found that SYVN1, an E3 ubiquitin ligase on the ER membrane, regulates ER shape and COPII exporting by mediating ubiquitination on ATLs, especially ATL1. ATL1 is ubiquitinated by SYVN1 strongly on K285 and mildly on K287. Ubiquitination on ATL1 does not result in protein degradation but inhibits ATL1 GTPase activity. *SYVN1* overexpression compensates the excessive ER network fusion caused by *ATL1* overexpression. Accordingly, the role of SYVN1 and ATL1 in regulating ER morphology is also recapitulated in *Caenorhabditis elegans*. Taken together, our study reveals a different role of SYVN1 in ER remodeling through mediating ubiquitination on ATLs.

INTRODUCTION

The endoplasmic reticulum (ER), extending from nuclear envelope to cell membrane, is one of the largest and the most complicated organelles in the eukaryotic cell. From nuclear envelope to the edge of cell, the type of ER membrane formation is divided into sheets and tubules. The sheets appear highly in ER homotypic membrane fusion, whereas the tubules display clearly in the form of network structure (Shibata et al., 2006; Westrate et al., 2015). High membrane curvature of ER tubules is generated by two classes of conserved ER membrane proteins, the Reticulons (RTNs) and REEPs/Yop1p, dominantly in the peripheral ER (Voeltz et al., 2006). It was reported that by reconstituting these proteins *in vitro*, they can form tubules in the 2D petri dishes, suggesting that they are the fundamental composition of ER structure (Hu et al., 2008; Voeltz et al., 2006). After that, more proteins have been identified in shaping the ER structure. Lunapark (LNPK) has been reported as a new conserved ER membrane protein required for maintaining the ER network (Chen et al., 2012). LNPK works synergistically with RTNs and REEPs/Yop1 to generate the three-way junctions on the ER network (Chen et al., 2012, 2015, 2013; Zhao et al., 2016). On the other hand, Atlastins (ATLs) antagonize LNPK to help homotypic membrane fusion in the ER-shaping process (Chen et al., 2012, 2013; Hu et al., 2009; Orso et al., 2009). LNPK and ATLs function together to maintain the dynamics of ER network.

There are three ATL members (ATL1, ATL2, and ATL3) in mammals, and they have different tissue-specific expression pattern despite their high sequence homology. ATL1 is highly expressed in brain, whereas ATL2 and ATL3 are extensively expressed in different tissues (Rismanchi et al., 2008). All three proteins mediate membrane fusion with different capacities, for ATL1 is the major one, whereas ATL2 and ATL3 play minor roles (Hu et al., 2009; O'Donnell et al., 2017). ER morphology is mildly affected by loss of ATL3 alone, and the phenotype resulting from loss of both ATL2 and ATL3 is rescued by ATL1 in the COS7 cell line (Hu et al., 2015). In addition, about 40 ATL1 mutations were identified from patients with hereditary spastic paraplegia (HSP), a neurodegenerative disease impairing motor neuron function of the cortical spinal tract (Ivanova et al., 2007; McCorquodale et al., 2011; Zhao et al., 2001).

SYVN1 is an ER-localized multispanning RING-finger ubiquitin ligase and participates in ER-associated protein degradation (ERAD) to degrade misfolded and unfolded proteins (Christianson and Ye, 2014; Smith et al., 2011; Vembar and Brodsky, 2008). SYVN1 has been reported to function as a channel that translocates

[1]School of Life Science and Technology, ShanghaiTech University, Shanghai 201210, China

[2]CAS Center for Excellence in Molecular Cell Science, Shanghai Institute of Biochemistry and Cell Biology, Chinese Academy of Sciences, Shanghai 200031, China

[3]Institute of Neuroscience and State Key Laboratory of Neuroscience, CAS Center for Excellence in Brain Science and Intelligence Technology, Chinese Academy of Sciences, Shanghai 200031, China

[4]University of Chinese Academy of Sciences, Beijing 100049, China

[5]These authors contributed equally

[6]Lead Contact

*Correspondence: zouyan@shanghaitech.edu.cn (Y.Z.), liuyf@shanghaitech.edu.cn (Y.L.)

https://doi.org/10.1016/j.isci.2020.101494

ERAD substrates containing misfolded segments into the cytosolic side (Baldridge and Rapoport, 2016). It has been reported that SYVN1 functions consequently with another ER-localized E3 ubiquitin ligase AMFR to help degrade ERAD substrates (Zhang et al., 2015). *SYVN1* is located on chromosome 11q13.1, a region where a deletion is found to link SPOAN syndrome, a neurodegenerative disorder mainly characterized by spastic paraplegia, optic atrophy, and neuropathy (SPOAN) (Macedo-Souza et al., 2005, 2009; Melo et al., 2015).

ATL1 promotes ER network formation by mediating homotypic membrane fusion, but how ATL1 itself is regulated under the dynamic cellular environment is not clear. Here by using genetic and biochemical approaches, we found that SYVN1 participates in ER remodeling and cargo sorting through ubiquitination regulation on ATLs. Overexpression of *ATL1* results in excessive fusion of ER network, converting tubular domain into sheet-like structure. Interestingly, overexpression of *SYVN1* compensates the phenotype of excessive fusion caused by *ATL1*. Further mapping analysis identified the two major ubiquitination sites K285 and K287 on ATL1 by SYVN1. Ubiquitination of ATL1 on these two residues inhibits its GTPase activity. *In vivo* experiments showed that the phenomena are also reproducible in *Caenorhabditis elegans* (*C. elegans*). Overexpression of *atln-1* (*ATL1* orthologue) in *C. elegans* motor neurons leads to abnormal distribution of ER network in axon, which is rescued by co-expression of *sel-11* (*SYVN1* orthologue). Collectively, we have identified SYVN1 ubiquitinates ATL1 to regulate ATL1 GTPase activity and participates in ER remodeling.

RESULTS

SYVN1 Is an E3 Ubiquitin Ligase for ATLs

There are multiple E3 ubiquitin ligases localized to the ER membrane (El Khouri et al., 2013; Neutzner et al., 2011). Given that ER is a dynamic network and constantly undergoing remodeling, we questioned whether the ER-localized E3 ubiquitin ligases participate in the regulation. To test this, we utilized the ER structural protein ATL1 to screen these E3 ubiquitin ligases that could interact with it. N-terminal MYC- or Flag-tagged ATL1 was used to immunoprecipitate or pull down the successfully expressed E3 ubiquitin ligases, which include MARCHF3, RNF185, AMFR, and SYVN1. The result showed that RNF185, AMFR, and SYVN1, as well as two cytosolic E3 ubiquitin ligases STUB1 and PJA1, all interacted with ATL1 (Figure S1A and S1B). Interestingly, the cell-based ubiquitination assay result revealed that only SYVN1 clearly simulated the ubiquitination modification on ATL1 (Figures 1A, S1C, and S1D). SYVN1 is a well-known E3 ubiquitin ligase that functions in ERAD to help misfolded protein degradation. Previous studies reported that SYVN1 functions parallel with another E3 ubiquitin ligase AMFR during ERAD (Zhang et al., 2015). We then used AMFR as the control of SYVN1. Consistent with the screening results, *SYVN1* knockdown reduced the ubiquitination level of ATL1, whereas *AMFR* knockdown had no influence on that (Figure 1B). Therefore, we conclude that SYVN1 is the E3 ubiquitin ligase specifically for ATL1. The endogenous interaction of SYVN1 and ATL1 was further verified by the co-immunoprecipitation using an anti-SYVN1 antibody (Figure 1C).

ATL family has three members—ATL1, ATL2, and ATL3—in human cells, and they have high sequence homology to each other (Figure 1D). When they were fused with MYC tag and transfected individually into cells, all of them were detected to interact with SYVN1 by the MYC immunoprecipitation assay (Figure 1E). We then examined whether all of them could be ubiquitinated by SYVN1. Interestingly, the cell-based ubiquitination assay indicated that ATL1 and ATL2 were robustly ubiquitinated, whereas ATL3 was slightly modified by SYVN1 (Figure 1F). Thereafter, we mainly focused on ATL1, the major ubiquitinated ATL by SYVN1, to investigate how it is regulated during ER remodeling process. We further generated an *ATL1* knock-in cell line, in which a FLAG tag was inserted at the C-terminus of *ATL1* ORF. However, we could only detect the Flag signal by western blotting but not by immunoprecipitation. Therefore, we relied on the exogenous ATLs for the cell-based assays.

SYVN1 Inhibits ER Homotypic Fusion and Restrains ER Sorting Capacity

Because ATL1 is a key player in ER morphogenesis, we questioned whether SYVN1, an E3 ubiquitin ligase of ATL1, is also involved in ER shaping. It was reported previously that different *ATL1* expression levels result in different ER morphology (Hu et al., 2009; Orso et al., 2009; Rismanchi et al., 2008; Wang et al., 2016). In our study, we used overexpressed *ATL1* to better indicate its function of inducing ER homotypic fusion. In this way, it is easy to screen out the genes that compromise the excessive fusion. As expected, compared with the control, the ER morphology was totally converted into sheet-like structure in *ATL1*-overexpressing cells, as indicated by SEC61B-GFP (Figure 2A). On the other hand, the ER structure in *SYVN1*-

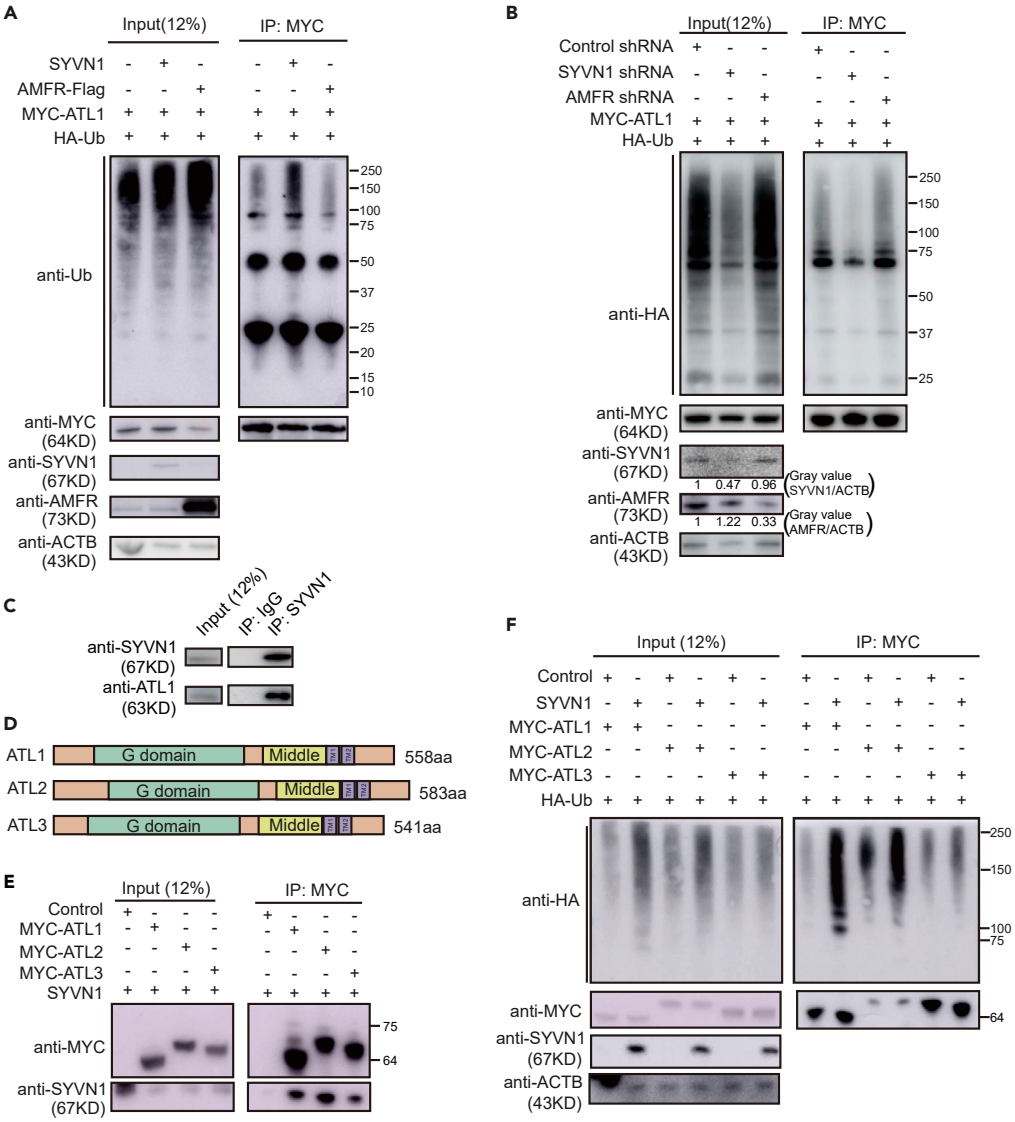

Figure 1. SYVN1 Interacts and Ubiquitinates ATL Family Members

(A) *MYC-ATL1* and the control or *SYVN1* or *Flag-AMFR*, together with *HA-ubiquitin* were co-transfected into HEK293FT cells. Immunoprecipitation under denaturing condition with anti-MYC beads was performed, and the samples were analyzed by immunoblotting.

(B) *MYC-ATL1* and *HA-ubiquitin*, along with the control shRNA, or *SYVN1* shRNA, or *AMFR* shRNA, were co-transfected into HEK293FT cells. After immunoprecipitation under denaturing condition with anti-MYC beads, samples were analyzed by immunoblotting. The knockdown efficiency of *SYVN1* and *AMFR* was labeled under the blots.

(C) Endogenous ATL1 interacts with SYVN1 in cells. Immunoprecipitation using either immunoglobulin G (IgG) or an anti-SYVN1 antibody was performed. The co-immunoprecipitated ATL1 was immunoblotted with an anti-ATL1 antibody.

(D) Schematic sequence of the three ATL family members. G domain means GTPase-containing region; TM means transmembrane domain.

(E) HEK293FT cells were transfected with *SYVN1* and *MYC-ATLs*. After 24 h, cells were lysed and immunoprecipitated with anti-MYC beads. The samples were analyzed by immunoblotting with the indicated antibodies.

(F) HEK293FT cells transfected with *MYC-ATLs* and *HA-ubiquitin*, along with the control or *SYVN1*. After 24 h, cells were immunoprecipitated with anti-MYC beads under denaturing condition. The samples were analyzed by immunoblotting with the indicated antibodies.

See also Figure S1.

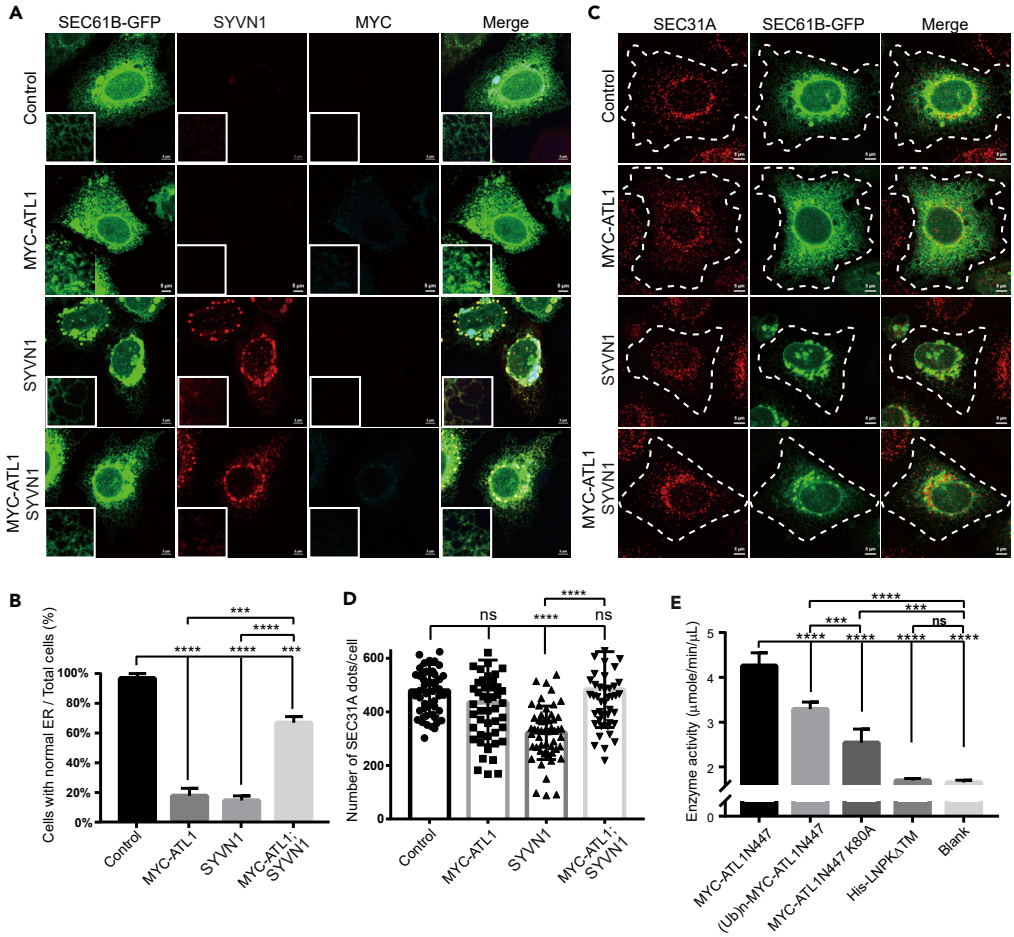

Figure 2. SYVN1 Inhibits ER Homotypic Fusion and Restrains COPII Exporting Capacity

(A) Representative images of HeLa cells transfected with the control, or *MYC-ATL1*, or/and *SYVN1* together with the ER marker *SEC61B-GFP*. After 24 h, cells were immunostained with the indicated antibodies. Scale bar, 5 μm.

(B) The statistical analysis of the samples in (A) shows the ratio of cells with normal ER network. Data are represented as mean ± SD from three independent experiments. About 100 cells were counted in each group. ***$p < 0.001$; ****$p < 0.0001$ (one-sided ANOVA).

(C) Representative images of HeLa cells transfected with the control, or *MYC-ATL1*, or/and *SYVN1* together with the ER marker *SEC61B-GFP*. After 24 h, cells were immunostained with SEC31A antibody to label COPII vesicles. Scale bar, 5 μm.

(D) The statistical analysis of the samples in (C) shows the number of SEC31A positive dots per cells under different transfected conditions. Data are represented as mean ± SD from three independent experiments. About 150 cells were counted in each group. ns, not significant; ****$p < 0.0001$ (one-sided ANOVA).

(E) GTPase activity of MYC-ATL1N447 and ubiquitinated MYC-ATL1N447. Bacterial purified MYC-ATL1N447 was first incubated with E1-GST, untagged UBE2D2, His-HA-ubiquitin for the ubiquitination reaction at 37°C for 1 h. Purified $(His\text{-}HA\text{-}ub)_n$-MYC-ATL1 and other proteins were then applied for the GTPase activity assay. MYC-ATL1N447 K80A and His-LNPKΔTM were used as negative controls. Data were represented as mean ± SD from three independent experiments. ns, not significant; ***$p < 0.001$; ****$p < 0.0001$ (one-sided ANOVA).

See also Figure S2.

overexpressing cells showed condensed pattern in the perinuclear region and high frequency of network disruption in the peripheral area (Figure 2A). Because ATL1 is the substrate of SYVN1, we surmised that *SYVN1* overexpression will compensate the overdose effect caused by *ATL1* overexpression. As anticipated, cells co-expressing *SYVN1* and *ATL1* partially recovered the ER structure back to normal (Figures 2A and 2B). These data implied that SYVN1 may regulate ER morphology through ubiquitination regulation on ATL1.

Next, we sought to determine whether the E3 ubiquitin ligase activity of SYVN1 plays a role in ER remodeling. HeLa cells were transiently transfected with *SYVN1* or the RING domain mutant *SYVN1 C329S*. Compared with the cells overexpressing *SYVN1*, in which the ER network was clearly disrupted, cells overexpressing *SYVN1 C329S* had less abnormal cell population (Figures S2A–S2C). From these results, we conclude that SYVN1 mediates the ubiquitination on ATL1, and its E3 ubiquitin ligase activity contributes to ER shaping.

To understand the physiological consequence of this dynamics, we employed a cell-based assay to analyze how SYVN1 regulation on ATL1 may influence the ER function. ATL1 was recently reported to help membrane trafficking and mediate COPII exporting from ER (Niu et al., 2019). We therefore examined whether this process is mediated by SYVN1 and ATL1. SEC31A is one of the subunits located on the surface of mature COPII vesicles and is a suitable marker for labeling the COPII vesicles. Immunostaining with an anti-SEC31A antibody showed numerous puncta structure in the perinuclear and peripheral area, which represented the exported COPII vesicles (Figure 2C). As shown, the number of SEC31A puncta in *ATL1*-overexpressing cells was similar to that of the control cells, whereas it was dramatically decreased by 30% in *SYVN1*-overexpressing cells (Figures 2C and 2D). Interestingly, when both *ATL1* and *SYVN1* were overexpressed, the puncta number was restored back to the control level (Figures 2C and 2D). This result is consistent with the ER morphology change mediated by SYVN1 and ATL1. Therefore, we conclude that SYVN1 and ATL1 regulate ER remodeling and control ER sorting signal pathway.

SYVN1 Is an E3 Ubiquitin Ligase for ATL1 Both in Cells and *In Vitro*

To further validate SYVN1 ubiquitination on ATL1 in cell, we first characterized which domain of ATL1 is responsible for the interaction with SYVN1. A series of truncations of ATL1 fused with FLAG tag was made to perform the pull-down assay. It showed that with the decrease of the truncation length, the N-terminal 309 amino acids (1-309aa) still interacted with SYVN1 (Figures 3A and 3B). Interestingly, truncation 1-309aa could still be ubiquitinated by SYVN1, although the level was lower than that of full-length ATL1 (Figure S3A).The C-terminal truncation 311-558aa could bind to SYVN1, whereas the truncation 450-558aa barely interacted with SYVN1. Therefore, both the G and Middle domains are essential for the interaction with SYVN1.

To exclude any other E3 ubiquitin ligase that might interfere with SYVN1 to ubiquitinate ATL1, we performed a ubiquitination assay under denaturing condition. The immunoblotting result showed that only SYVN1, but not SYVN1 C329S mutant, succeeded to build ubiquitin chain on ATL1 in cells (Figure 3C). The result also verified that SYVN1 is a specific E3 ubiquitin ligase for ATL1. The classical E2 that conjugates SYVN1 for protein degradation in ERAD pathway is UBE2G2 (Kikkert et al., 2004), so we tested whether this is the E2 for SYVN1 to ubiquitinate ATL1. We also included another E2 UBE2D2, which is a widely used E2 enzyme for *in vitro* E3 ubiquitin ligase activity assays (Lorick et al., 2005). Different from UBE2G2, UBE2D2 does not form specific Lys48-linked ubiquitin chains on substrate for proteasome degradation (Kikkert et al., 2004). To our surprise, UBE2G2 failed to form ubiquitin chain on the recombinant N-terminal cytosolic segment Flag-ATL1N447 (1-447aa), whereas UBE2D2 nicely spurred the ubiquitin chain formation on the substrate (Figure S3B). These data implied that ATL1 is not a conventional ERAD substrate, and the ubiquitination modification on ATL1 by SYVN1 may regulate ATL1 function. Next, we aimed to verify this result by using the full-length ATL1. The ubiquitination assay was performed by combining E1, the general E2 UBE2D2, recombinant GST-tagged cytosolic SYVN1, and ubiquitin, together with the mammalian purified MYC-ATL1. An immunoprecipitation under denaturing condition was followed to exclude any non-covalent associated ubiquitin. The immunoblotting result clearly showed that MYC-ATL1 was robustly ubiquitinated by SYVN1 (Figure 3D). The catalytic inactivated mutant SYVN1 C329S was not able to conjugate ubiquitin on MYC-ATL1, neither did another ER-anchored E3 ubiquitin ligase RNF185 (Figure 3D). Furthermore, when the mammalian purified ATL1 was substituted by a bacteria-derived recombinant N-terminal cytosolic segment MYC-ATL1N447 (1-447aa), the same result was obtained (Figure 3E). Therefore, our data indicated that SYVN1 is a bona fide ubiquitin ligase for ATL1 both in cells and *in vitro*.

Interestingly, we found ATL2 was also ubiquitinated by SYVN1 but not SYVN1 mutant *in vitro* (Figure S3C). However, the ubiquitination level of MYC-ATL2 was about the same in *SYVN1*-overexpressing cells as that in *SYVN1 C329S*-overexpressing cells (Figure S3D). These results implied that although ATL2 is ubiquitinated by SYVN1 similar to ATL1, there might be other E3 ubiquitin ligase that also controls the ubiquitination status of ATL2 in cells. To validate the discrepancy of the three ATLs, an *in vitro* ubiquitination assay was performed using the recombinant N-terminal cytosolic segments of ATLs. We observed that ATL1,

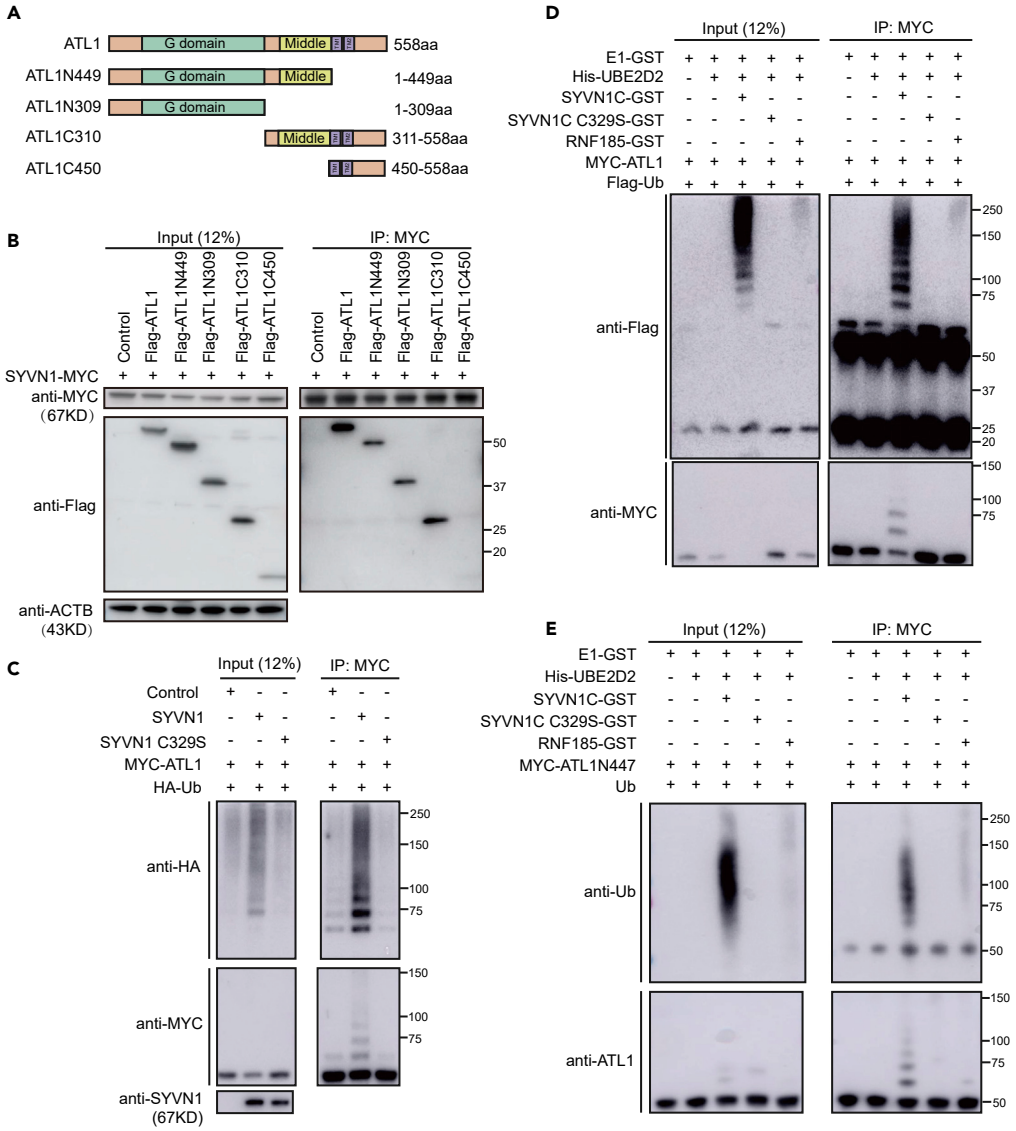

Figure 3. SYVN1 Ubiquitinates ATL1 in Cell and *In Vitro*

(A) A series of ATL1 truncation mutants were made based on the domain structure of ATL1.

(B) *SYVN1-MYC* and *Flag-ATL1* or its truncations were co-transfected into HEK295FT cells. After 24 h, cells were lysed and immunoprecipitated with anti-MYC beads. The samples were analyzed by immunoblotting.

(C) *MYC-ATL1*, *HA-ubiquitin*, and *SYVN1* or *SYVN1C329S* were co-transfected into HEK293FT cells. After 24 h, immunoprecipitation under denaturing condition with anti-MYC beads was performed. Ubiquitinated MYC-ATL1 was analyzed by immunoblotting.

(D) Mammalian purified MYC-ATL1 was incubated with E1-GST, His-UBE2D2, Flag-ubiquitin, together with SYVN1C-GST or SYVN1C C329S-GST or RNF185-GST for 1 h at 37°C. Immunoprecipitation under denaturing condition with anti-MYC beads was performed, and ubiquitinated MYC-ATL1 was analyzed by immunoblotting.

(E) As (D), except using recombinant protein MYC-ATL1N447 and untagged ubiquitin purified from bacteria.

See also Figure S3.

ATL2, and only slight amount of ATL3 were ubiquitinated by SYVN1 (Figure S3E). The discrepancy might be caused by the subtle sequence difference among ATLs.

To see whether ATL1 ubiquitination by SYVN1 affects its GTPase activity, we performed an *in vitro* GTPase activity assay. Bacterial purified recombinant protein MYC-ATL1N447 was first incubated with E1,

untagged UBE2D2, recombinant GST-tagged cytosolic SYVN1, and His-ubiquitin for the ubiquitination assay. The ubiquitinated MYC-ATL1N447 was then collected by Ni Sepharose and eluted by imidazole. After buffer exchange and removal of the free ubiquitin, the amount of ubiquitinated MYC-ATL1N447 for the GTPase activity assay was normalized to that of the control proteins as shown in the Coomassie staining result (Figure S3F). Compared with that of ATL1N447, the GTPase activity of the ubiquitinated ATL1N447 was significantly reduced (Figure 2E). ATL1N447K80A is a GTPase-deficient mutant (Rismanchi et al., 2008) and was served as a negative control. The ER structural protein LNPK (His-tagged LNPK excluding the transmembrane domains) was also used as a negative control. From these data we conclude that the GTPase activity of ATL1 is decreased when ATL1 is ubiquitinated by SYVN1.

ER Network Regulation Is Dependent on the E3 Ubiquitin Ligase Activity of SYVN1

The above data demonstrate that SYVN1 ubiquitinates ATL1, and the two proteins have opposite roles in ER remodeling. To see whether SYVN1 regulating ER remodeling is dependent on its ligase activity, we examined the ER morphology under different forms of SYVN1. Compared with *ATL1* and *SYVN1* co-expression, which partially compensated the defect caused by *ATL1* overexpression, co-expression of *ATL1* and *SYVN1 C329S* did not relieve the excessive fusion caused by *ATL1* overexpression (Figures 4, S4A, and S4B).

Previous studies have shown that *ATL1* mutants or GTP-absence could induce ER homotypic fusion deficiency (Hu et al., 2009; Orso et al., 2009; Rismanchi et al., 2008). And we observed a similar phenotype in *ATL1* knockdown cells (Figures S4C and S4D). In contrast, knockdown of *SYVN1* caused ER network fusion resembling to the effect of *ATL1* overexpression (Figures S4C and S4D). The ER network in *ATL1* and *SYVN1* double knockdown was partially rescued from excessive fusion (Figures S4C and S4D). In conclusion, these findings demonstrate that SYVN1 and ATL1 cooperatively regulate ER dynamics.

ATL1 K285 and K287 Are the Major Ubiquitination Sites Modified by SYVN1

To identify the ubiquitination sites on ATL1 modified by SYVN1, we performed the ubiquitination assay as that in Figure 3E using MYC-ATL1N447 as the substrate and applied the MYC immunoprecipitated samples for mass spectrometry analysis. A total of 13 lysine residues on ATL1 were identified, with an increase of the ubiquitination signal in the presence of SYVN1 (Table S1). Among these 13 residues, there are seven residues (K30, K80, K234, K238, K285, K287, and K319) with an increase of the ubiquitin signal from zero in the control to a significantly high level in *SYVN1*-treated condition (Table S1). The other two candidates are K241, having the highest increase of the ubiquitination signal, and K41, located close to the ATL1 GTPase pocket (Figure S5A). We then mutated these lysine residues to alanine in *MYC-ATL1* individually and co-expressed the mutants with *SYVN1* in cells to examine the change of the ubiquitination level. After immunoprecipitation under denaturing condition, the immunoblotting result showed that the two mutants K285A and K287A largely abolished the ubiquitination signal, with K285A mutant the most significantly. The other mutants showed a similar level of ubiquitination modification to that of wild-type MYC-ATL1 (Figure S5B). *In vitro* ubiquitination assay by incubating bacterial purified N-terminal cytosolic segment MYC-ATL1N447 or the mutant proteins together with E1, UBE2D2, SYVN1, and ubiquitin further verified that K285 and K287 were the major ubiquitinated sites by SYVN1 (Figure 5A). Furthermore, the double mutant MYC-ATL1N447 K285A/K287A was barely modified by SYVN1 (Figure 5A). The GTPase activity of the double mutant MYC-ATL1N447 K285A/K287A was not affected (Figure S5C). K285 and K287 happen to be in the spatial position that is close to the GTPase pocket and the dimerization site of the two monomers (Bian et al., 2011; Byrnes et al., 2013; Byrnes and Sondermann, 2011) (Figure S5A), implying that ubiquitination on these two residues may interfere with ATL1 dimerization and/or its GTPase activity.

We next examined how these mutants affect ER remodeling in cells. We observed that overexpression of *K285A*, *K287A*, or *K285A/K287A* exhibited excessive fusion of ER network similar to that of overexpression of wild-type *MYC-ATL1* (Figures 5B, 5C, S6A, and S6B). Interestingly, SYVN1 rescued the excessive fusion caused by wild-type *MYC-ATL1* but not *K285A* or *K285A/K287A* mutant (Figures 5B and 5C). The phenotype of *K287A* overexpression, however, was partial rescued by SYVN1 (Figures 5C, S6A and S6B). These data further support that SYVN1 participates in ER remodeling through ubiquitination regulation on ATL1.

The Motor Neuronal ER Morphology Is Regulated by *atln-1* and *sel-11* in *C. elegans*

Next we aimed to check whether SYVN1 and ATL1 have a similar regulation *in vivo*. It has been reported that *ATL1* mutants or deficiency not only dysregulates ER homotypic fusion but also highly links to a neurodegenerative disease named hereditary spastic paraplegia (HSP) in human (Guelly et al., 2011). HSP is

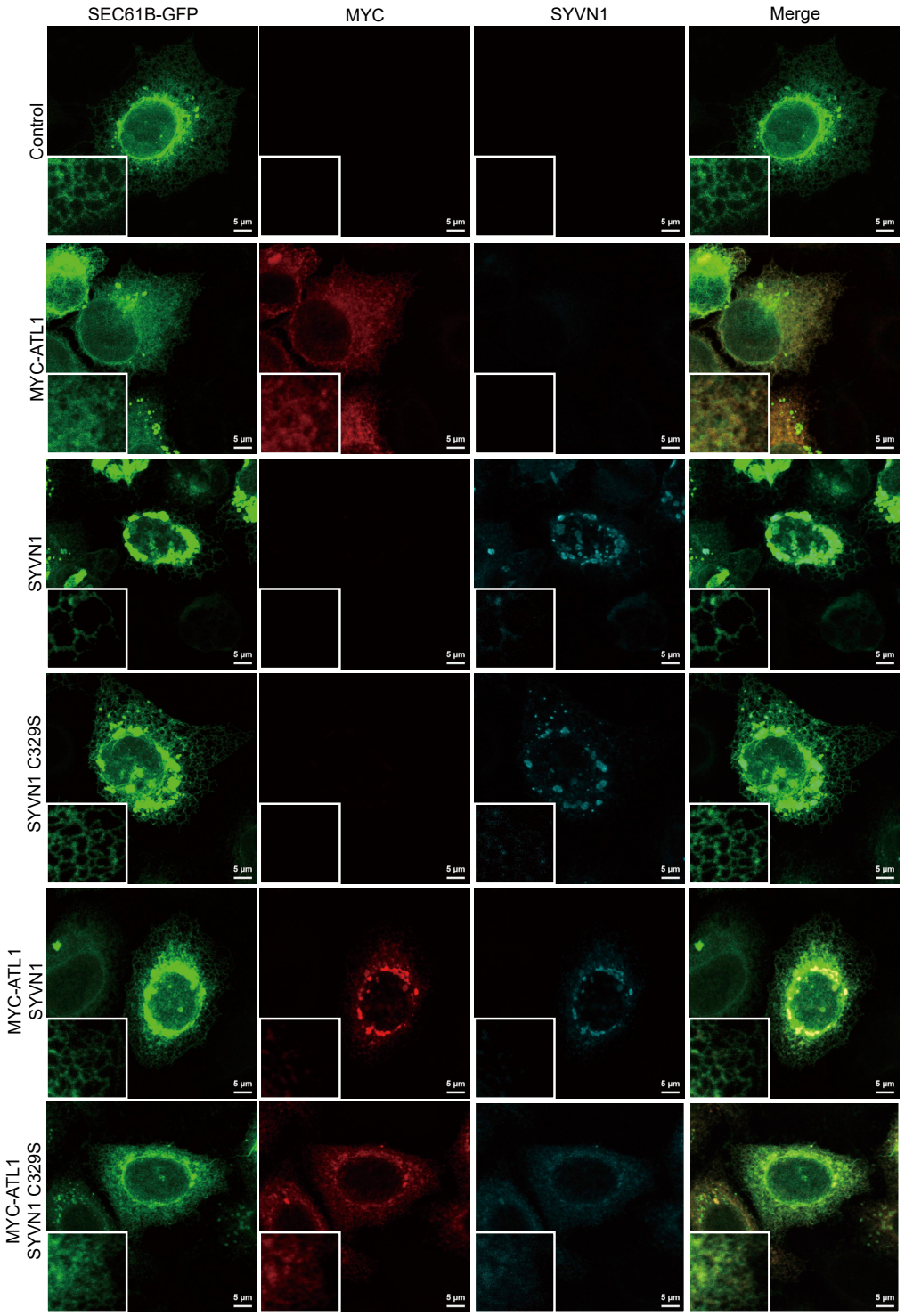

Figure 4. ER Network Remodeling Is Dependent on the E3 Ubiquitin Ligase Activity of SYVN1

Representative images of HeLa cells transfected with the control, or *MYC-ATL1*, or/and *SYVN1*, or/and *SYVN1C329S*, together with the ER marker *SEC61B-GFP*. After 24 h, cells were fixed and stained with the indicated antibodies. Scale bar, 5 μm. Refer to Figure S4B for the statistical analysis.

See also Figure S4.

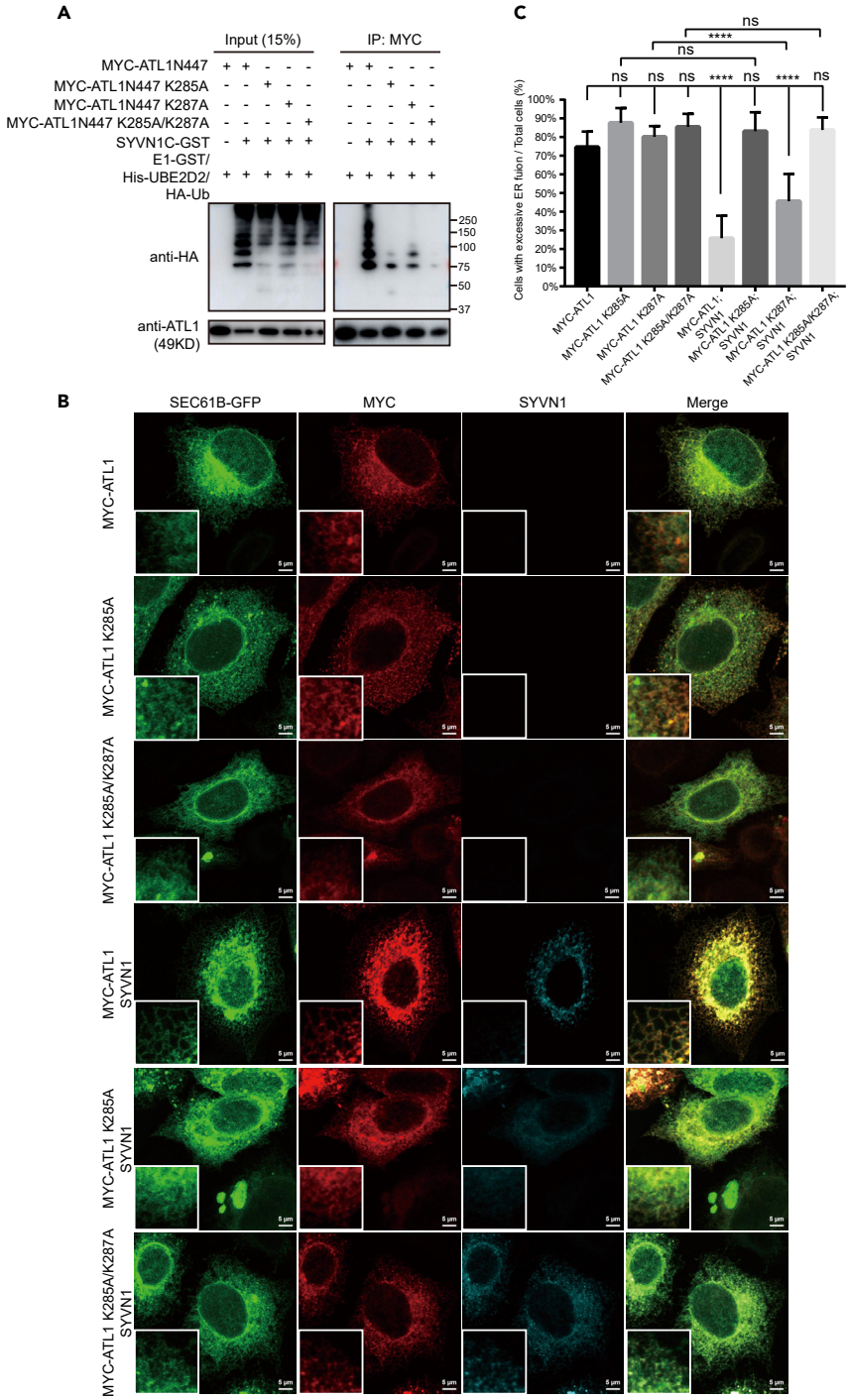

Figure 5. SYVN1 Ubiquitinates ATL1 Mainly on K285 and K287

(A) E1-GST, His-UBE2D2, HA-ubiquitin, SYVN1C-GST, and bacterial purified recombinant MYC-ATL1N447 or its mutants were incubated at 37°C for 1 h. The reaction samples were then immunoprecipitated under denaturing condition with anti-MYC Beads. All samples were analyzed by immunoblotting.

(B) Representative images of HeLa cells transfected with the control, or *MYC-ATL1*, or *MYC-ATL1 K285A* or *MYC-ATL1 K285A/K287A*, along with the control or *SYVN1*, together with the ER marker *SEC61B-GFP*. After 24 h, cells were fixed and immunostained with the indicated antibodies. Scale bar, 5 μm.

Figure 5. *Continued*
(C) The statistical analysis of samples in (B) and Figure S6A shows the ratio of cells with excessive ER fusion. Data are represented as mean ± SD from three independent experiments. About 100 cells were counted in each group. ns, not significant; ****p < 0.0001 (one-sided ANOVA).
See also Figures S5 and S6 and Table S1.

mostly caused by dysfunction of the motor neurons in human. Therefore, we aimed to test the motor neuron function in *C. elegans*. TRAM-1 is mainly localized to rough ER; therefore, it is often used as an ER marker (Rolls et al., 2002). A *C. elegans* strain stably expressing TRAM-1 in motor neurons named BLW559 (*ybqIs55[flp-13p::tagRFP::tram-1])* was used to visualize ER morphology in worms (Meng et al., 2017). The distribution of ER network in motor neurons was very unique for the rough ER mostly existed in the cell body (Figure 6A WT). To better trace the change of the ER structure, the motor neurons were highlighted with GFP, which was driven by a motor neuron-specific promoter *flp-13p* and exclusively expressed in these neurons (*Ex[Flp-13p::GFP]*) (Figure 6A WT). We first overexpressed *ATL1* orthologue gene *atln-1* in neurons of the worm driven by a neuron-specific promoter *rgef-1*. Similar to that observed in the cell line, we found that high level of *atln-1* induced abnormal distribution of ER network extending from the cell body to the axons (Figure 6A, WT versus Ex[*rgef-1p::atln-1*]). On the contrast, when we overexpressed the *SYVN1* orthologue gene *sel-11* in neurons, the ER distribution in the motor neurons was reduced to the cell body but barely in the axon (Figure 6A, WT versus Ex[*rgef-1p::sel-11*]). The *sel-11C295Y* (a dysfunctional RING domain mutation) (Choi et al., 2010) had no observable change of the ER morphology compared with the wild type. Co-expression of *atln-1* and *sel-11* counteracted the phenotype with a normal ER distribution. However, overexpression of *sel-11C295Y* could not rescue the ER morphology abnormality caused by excessive expression of *atln-1* (Figures 6A–6C).

We also introduced two mutant strains, *atln-1(yan24)* (*atln-1* KO mutant) and *sel-11(ar39)* (*sel-11* dysfunctional RING domain mutant), and found that *atln-1* could compensate the deficiency caused by *sel-11* (Figures 6D and 6E). The ER distribution in *atln-1* was reduced to just the cell body with marginal amount in axons (Figure 6D). On the other hand, *sel-11* showed obvious abnormal ER distribution in motor neurons, for large amount of TRAM-1 extended to the axons, specifically in the first two motor neurons (Figure 6D). Interestingly, we found that *atln-1* had a critical impact in decreasing the degree of abnormal ER distribution induced by *sel-11* (Figure 6D). The statistical results also supported the phenotype we have found (Figure 6E). These data are consistent with the findings we have observed in cell lines (Figures 4 and S4C). Together, we identified that SYVN1/SEL-11 antagonizes ATL1/ATLN-1 to regulate the ER network both in cells and in *C. elegans*.

Because *ATL1* mutant or deficiency is related to HSP disease, we examined whether *atln-1* could also affect worm mobility. Interestingly, we found that *atln-1* showed noticeable mobility dysfunction (Figure S7A), but *sel-11* did not rescue this abnormality (Figures S7B and S7C). In addition, *atln-1* also appeared to have infertility problem. Taken together, we found that the ER morphology change could also be recapitulated in *C. elegans*. However, we need more data to verify whether *sel-11* plays a role in *atln-1* regulated motor neuron dysfunction in *C. elegans*.

DISCUSSION

In this study, we provided the evidence that SYVN1 regulates ER shaping in addition to its role as a classical E3 ubiquitin ligase of ERAD. Our mass spectrometry result and biochemical analysis showed that SYVN1 ubiquitinates ATL1, and ubiquitination on ATL1 inhibits its GTPase activity, which then represses ER homotypic membrane fusion. Therefore, we propose a model that SYVN1 balances ER remodeling via ubiquitination regulation on ATL1 (Figure 7).

SYVN1 is a well-studied E3 ubiquitin ligase that functions in ERAD (Christianson and Ye, 2014; Smith et al., 2011; Vembar and Brodsky, 2008). It typically ubiquitinates misfolded substrates from ER for degradation (Carvalho et al., 2010; Foresti et al., 2014; Khmelinskii et al., 2014). There is no report showing that substrates other than misfolded proteins from ER are ubiquitinated by SYVN1. Because ER is a highly dynamic organelle that is always remodeling depending on cellular demand, we surmised there might be regulators that keep this equilibrium. RTNs and REEPs/Yop1p are the constitutive components of the ER network formation (Voeltz et al., 2006), whereas ATLs are known to catalyze homotypic membrane fusion in the smooth ER to remodel ER (Hu et al., 2009; Liu et al., 2015; Orso et al., 2009). In our initial screening assay, among these ER structural proteins, we found that only ATL family members, but not RTNs, REEPs/Yop1p, or LNPK,

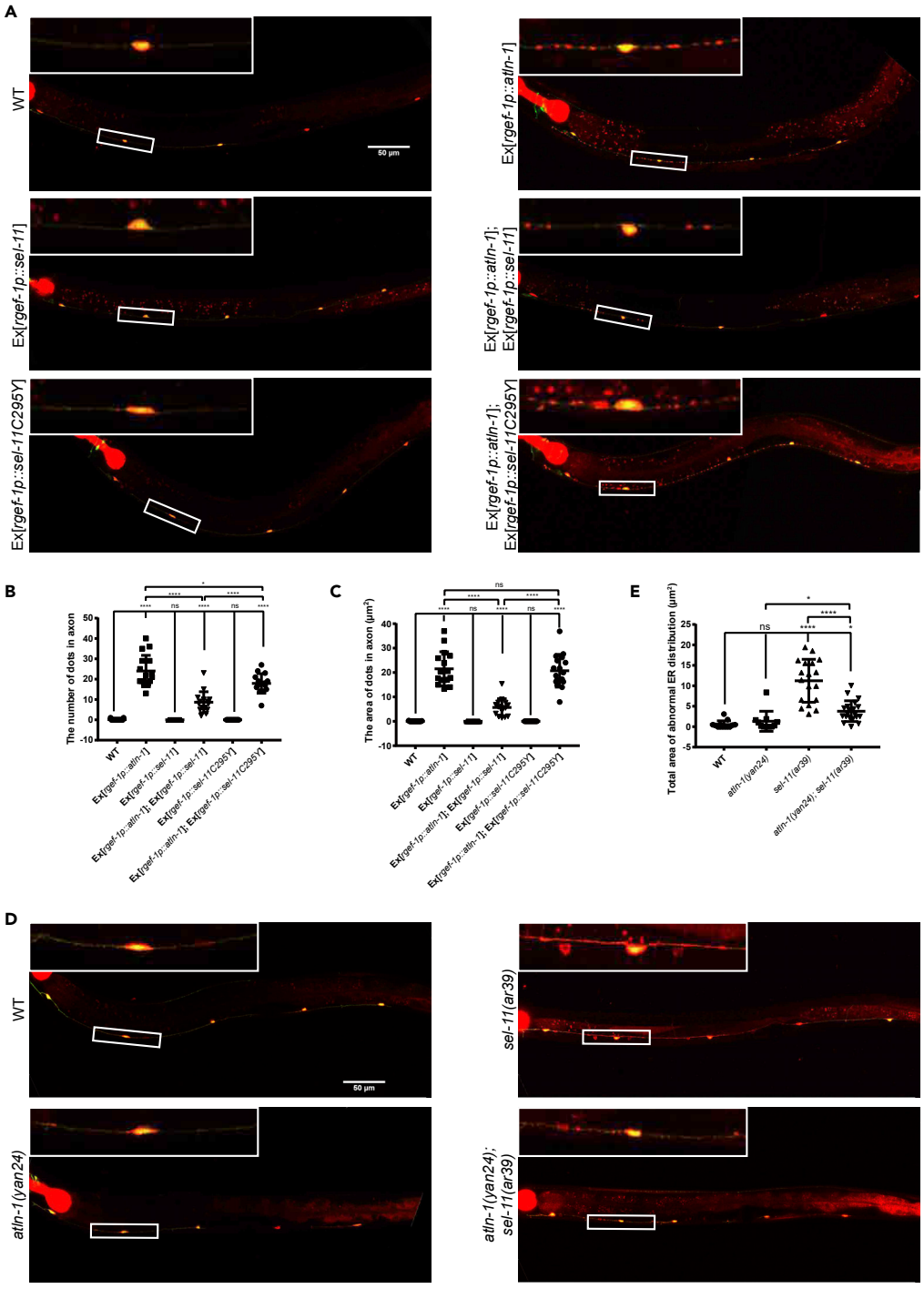

Figure 6. ATLN-1 and SEL-11 Regulate ER Morphology of the Motor Neurons in *C. elegans*

(A) Worms were photographed and analyzed by confocal microscope at L4 stage. The motor neurons were labeled with GFP by expressing the transgene *Ex[Flp-13p::GFP]*. The ER marker TRAM-1 was labeled with RFP by expressing the transgene *ybqIs55[flp-13p::tagRFP::tram-1]* in *C. elegans* motor neurons. The magnified region was chosen from the representative area on the motor neurons. Scale bar, 50 μm.

(B and C) The statistical analysis of the number and area of abnormal distributed puncta on axon of the motor neurons in (A). Data are represented as mean ± SD. About 10–20 worms were counted for each group. ns, not significant; *p < 0.05; ****p < 0.0001 (one-sided ANOVA).

Figure 6. *Continued*

(D) Wild-type strain and mutant *atln-1(yan24)*, *sel-11(ar39)* and *atln-1(yan24);sel-11(ar39)* were photographed and analyzed at L4 stage by confocal microscope. The motor neurons were labeled with GFP by expressing the transgene *Ex [Flp-13p::GFP]*. The ER marker TRAM-1 was labeled with RFP by expressing the transgene *ybqIs55[flp-13p::tagRFP::tram-1]* in *C. elegans* motor neurons. The magnified region was chosen from the representative area on the motor neurons. Scale bar, 50 μm.

(E) The statistical analysis of total area of abnormal distributed puncta on axon of the motor neurons in (D). Data are represented as mean ± SD. About 10–20 worms were counted for each group. ns, not significant; *p < 0.05; ****p < 0.0001 (one-sided ANOVA).

See also Figure S7.

were ubiquitinated by SYVN1. Interestingly, poly-ubiquitination of ATL1 by SYVN1 does not result in protein degradation. By further identification of the linkage type, our data suggested the ubiquitin chain formed on ATL1 might be a mixture of K27 and K29 (data not shown). K27- and K29-linked ubiquitin chains have been reported to modify LRRK2, which then leads to LRRK2 aggregation and neuronal protection in primary neurons and in a *Drosophila* model of LRRK2 G2019S (Nucifora et al., 2016). From the structural analysis of ATL1 N-terminal cytosolic domain (Bian et al., 2011; Byrnes et al., 2013; Byrnes and Sondermann, 2011), we noticed that the ubiquitination sites K285 and K287 on ATL1 are close to the ATL1 dimerization interface. Our ATL1 GTPase activity assay further supported the idea that ubiquitination of ATL1 inhibited GTPase activity (Figure 2E). The phenotype that *SYVN1* co-expressing with *ATL1 K285A* or *K285A/K287A* mutants could not rescue the excessive fusion further verified that ubiquitination of ATL1 interferes with ATL1 function (Figures 5B and 5C). Therefore, we proposed that poly ubiquitination on K285 and K287 by SYVN1 inhibits ATL1 dimerization and homotypic fusion of ER membranes.

It was reported previously that ATL1 antagonizes LNPK to regulate ER remodeling (Chen et al., 2012, 2015, 2013; Zhou et al., 2019). Here by identifying SYVN1 ubiquitinating on ATL1, we characterized another level of regulation by LNPK and ATLs. Therefore, SYVN1 is an intermediator to help balance between the ER structural proteins.

We also tested the role of SYVN1 and ATL1 in regulating ER morphology in *C. elegans*. The result showed that SYVN1 and ATL1 regulate ER network conservatively in *C. elegans* and human cells. As mutants or deficiency of *ATL1* has been proved to induce HSP (Ivanova et al., 2007; McCorquodale et al., 2011; Zhao et al., 2001), our data showed that *atln-1* mutant in worms also resulted in motor disturbance. However, the *atln-1;sel-11* mutant in worms did not rescue the motor disturbance significantly (Figures S7A–S7C). Although we could not exclude *sel-11* function in recovery of mobility disorder caused by *atln-1*, it is of certainty that *sel-11* functions together with *atln-1* in regulating ER morphology.

Therefore, our findings provide insight into how the ER dynamics is fine-tune regulated by SYVN1 via ubiquitination modification on ATLs, and this is recapitulated in *C. elegans*. Further crystal structure study on how ubiquitinated ATL1 affects its dimerization would be the next step.

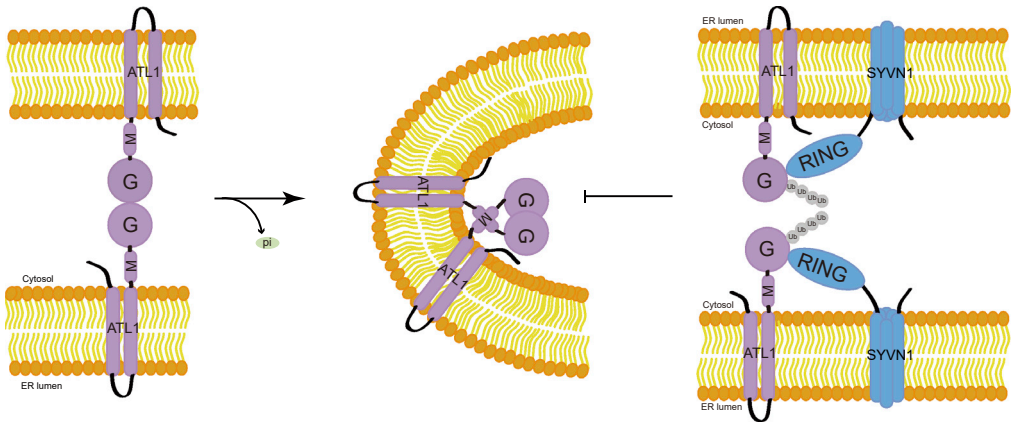

Figure 7. A Simple Model of SYVN1 Ubiquitinating ATL1 to Regulate ER Membrane Fusion

ATL1 promotes ER homotypic membrane fusion by hydrolyzing GTP. SYVN1 ubiquitinates ATL1 to inhibit ATL1 GTPase activity and therefore prevents membrane fusion.

Limitations of the Study

In this study, we reported that ER-shaping protein ATLs, particularly ATL1, can be ubiquitinated by ER-resident E3 ubiquitin ligase SYVN1, which in turn regulates ER morphology and functions. However, most of the experiments were done with overexpressed or purified proteins. Therefore, further functional study of how SYVN1 regulates ATLs at the endogenous level will be required in the next step.

Resource Availability

Lead Contact

Further information should be directed to and will be fulfilled by the Lead Contact, Yanfen Liu (liuyf@shanghaitech.edu.cn).

Materials Availability

Materials are available upon request from Dr. Yanfen Liu.

Data and Code Availability

This study did not generate/analyze datasets.

METHODS

All methods can be found in the accompanying Transparent Methods supplemental file.

SUPPLEMENTAL INFORMATION

Supplemental Information can be found online at https://doi.org/10.1016/j.isci.2020.101494.

ACKNOWLEDGMENTS

We thank Professor Junjie Hu (Chinese Academy of Sciences), Dr. Yihong Ye (National Institutes of Health, USA), Dr. Wei Li (Chinese Academy of Sciences), Dr. Cynthia Wolberger (John Hopkins University), Professor Kazuhiro Iwai (Kyoto University), Dr. Song Huang (National Institute of Biological Sciences, Beijing, China), and Dr. Jiahuai Han (Xiamen University) for constructs. Some strains were provided by Dr. Yingchuan Qi (ShanghaiTech University) and the CGC, which is funded by NIH Office of Research Infrastructure Programs (P40 OD010440). We thank the Image Core Facility at ShanghaiTech University for assisting with confocal microscopy. We thank Multi-omics Facility at ShanghaiTech University for sequencing and analyzing the samples. This study was supported by the National Natural Science Foundation of China (No. 31570781 and No. 31770831) and the Start-up grant from ShanghaiTech University. This study was also supported by the National Natural Science Foundation of China (No.31571047) from Y.Z.'s lab.

AUTHOR CONTRIBUTIONS

Y. Liu and Y. Zou designed the experiments and wrote the manuscript. Y. Zhao, Z. Feng, Y. Liu, and Y Zou performed the experiments and analyzed data.

DECLARATION OF INTERESTS

The authors declare no competing interests.

Received: February 10, 2020
Revised: July 1, 2020
Accepted: August 19, 2020
Published: September 25, 2020

REFERENCES

Baldridge, R.D., and Rapoport, T.A. (2016). Autoubiquitination of the Hrd1 ligase triggers protein retrotranslocation in ERAD. Cell *166*, 394–407.

Bian, X., Klemm, R.W., Liu, T.Y., Zhang, M., Sun, S., Sui, X., Liu, X., Rapoport, T.A., and Hu, J. (2011). Structures of the atlastin GTPase provide insight into homotypic fusion of endoplasmic reticulum membranes. Proc. Natl. Acad. Sci. U S A *108*, 3976–3981.

Byrnes, L.J., Singh, A., Szeto, K., Benvin, N.M., O'Donnell, J.P., Zipfel, W.R., and Sondermann, H. (2013). Structural basis for conformational switching and GTP loading of the large G protein atlastin. EMBO J. *32*, 369–384.

Byrnes, L.J., and Sondermann, H. (2011). Structural basis for the nucleotide-dependent dimerization of the large G protein atlastin-1/

SPG3A. Proc. Natl. Acad. Sci. U S A *108*, 2216–2221.

Carvalho, P., Stanley, A.M., and Rapoport, T.A. (2010). Retrotranslocation of a misfolded luminal ER protein by the ubiquitin-ligase Hrd1p. Cell *143*, 579–591.

Chen, S., Desai, T., McNew, J.A., Gerard, P., Novick, P.J., and Ferro-Novick, S. (2015). Lunapark stabilizes nascent three-way junctions in the endoplasmic reticulum. Proc. Natl. Acad. Sci. U S A *112*, 418–423.

Chen, S., Novick, P., and Ferro-Novick, S. (2012). ER network formation requires a balance of the dynamin-like GTPase Sey1p and the Lunapark family member Lnp1p. Nat. Cell Biol. *14*, 707–716.

Chen, S., Novick, P., and Ferro-Novick, S. (2013). ER structure and function. Curr. Opin. Cell Biol. *25*, 428–433.

Choi, M.S., Yoo, A.S., and Greenwald, I. (2010). sel-11 and cdc-42, two negative modulators of LIN-12/Notch activity in C. elegans. PLoS One *5*, e11885.

Christianson, J.C., and Ye, Y. (2014). Cleaning up in the endoplasmic reticulum: ubiquitin in charge. Nat. Struct. Mol. Biol. *21*, 325–335.

El Khouri, E., Le Pavec, G., Toledano, M.B., and Delaunay-Moisan, A. (2013). RNF185 is a novel E3 ligase of endoplasmic reticulum-associated degradation (ERAD) that targets cystic fibrosis transmembrane conductance regulator (CFTR). J. Biol. Chem. *288*, 31177–31191.

Foresti, O., Rodriguez-Vaello, V., Funaya, C., and Carvalho, P. (2014). Quality control of inner nuclear membrane proteins by the Asi complex. Science *346*, 751–755.

Guelly, C., Zhu, P.P., Leonardis, L., Papic, L., Zidar, J., Schabhuttl, M., Strohmaier, H., Weis, J., Strom, T.M., Baets, J., et al. (2011). Targeted high-throughput sequencing identifies mutations in atlastin-1 as a cause of hereditary sensory neuropathy type I. Am. J. Hum. Genet. *88*, 99–105.

Hu, J., Shibata, Y., Voss, C., Shemesh, T., Li, Z., Coughlin, M., Kozlov, M.M., Rapoport, T.A., and Prinz, W.A. (2008). Membrane proteins of the endoplasmic reticulum induce high-curvature tubules. Science *319*, 1247–1250.

Hu, J., Shibata, Y., Zhu, P.P., Voss, C., Rismanchi, N., Prinz, W.A., Rapoport, T.A., and Blackstone, C. (2009). A class of dynamin-like GTPases involved in the generation of the tubular ER network. Cell *138*, 549–561.

Hu, X., Wu, F., Sun, S., Yu, W., and Hu, J. (2015). Human atlastin GTPases mediate differentiated fusion of endoplasmic reticulum membranes. Protein Cell *6*, 307–311.

Ivanova, N., Claeys, K.G., Deconinck, T., Litvinenko, I., Jordanova, A., Auer-Grumbach, M., Haberlova, J., Lofgren, A., Smeyers, G., Nelis, E., et al. (2007). Hereditary spastic paraplegia 3A associated with axonal neuropathy. Arch. Neurol. *64*, 706–713.

Khmelinskii, A., Blaszczak, E., Pantazopoulou, M., Fischer, B., Omnus, D.J., Le Dez, G., Brossard, A., Gunnarsson, A., Barry, J.D., Meurer, M., et al. (2014). Protein quality control at the inner nuclear membrane. Nature *516*, 410–413.

Kikkert, M., Doolman, R., Dai, M., Avner, R., Hassink, G., van Voorden, S., Thanedar, S., Roitelman, J., Chau, V., and Wiertz, E. (2004). Human HRD1 is an E3 ubiquitin ligase involved in degradation of proteins from the endoplasmic reticulum. J. Biol. Chem. *279*, 3525–3534.

Liu, T.Y., Bian, X., Romano, F.B., Shemesh, T., Rapoport, T.A., and Hu, J. (2015). Cis and trans interactions between atlastin molecules during membrane fusion. Proc. Natl. Acad. Sci. U S A *112*, E1851–E1860.

Lorick, K.L., Jensen, J.P., and Weissman, A.M. (2005). Expression, purification, and properties of the Ubc4/5 family of E2 enzymes. Methods Enzymol. *398*, 54–68.

Macedo-Souza, L.I., Kok, F., Santos, S., Amorim, S.C., Starling, A., Nishimura, A., Lezirovitz, K., Lino, A.M., and Zatz, M. (2005). Spastic paraplegia, optic atrophy, and neuropathy is linked to chromosome 11q13. Ann. Neurol. *57*, 730–737.

Macedo-Souza, L.I., Kok, F., Santos, S., Licinio, L., Lezirovitz, K., Cavacana, N., Bueno, C., Amorim, S., Pessoa, A., Graciani, Z., et al. (2009). Spastic paraplegia, optic atrophy, and neuropathy: new observations, locus refinement, and exclusion of candidate genes. Ann. Hum. Genet. *73*, 382–387.

McCorquodale, D.S., 3rd, Ozomaro, U., Huang, J., Montenegro, G., Kushman, A., Citrigno, L., Price, J., Speziani, F., Pericak-Vance, M.A., and Zuchner, S. (2011). Mutation screening of spastin, atlastin, and REEP1 in hereditary spastic paraplegia. Clin. Genet. *79*, 523–530.

Melo, U.S., Macedo-Souza, L.I., Figueiredo, T., Muotri, A.R., Gleeson, J.G., Coux, G., Armas, P., Calcaterra, N.B., Kitajima, J.P., Amorim, S., et al. (2015). Overexpression of KLC2 due to a homozygous deletion in the non-coding region causes SPOAN syndrome. Hum. Mol. Genet. *24*, 6877–6885.

Meng, J., Ma, X., Tao, H., Jin, X., Witvliet, D., Mitchell, J., Zhu, M., Dong, M.Q., Zhen, M., Jin, Y., et al. (2017). Myrf ER-bound transcription factors drive C. elegans synaptic plasticity via cleavage-dependent nuclear translocation. Dev. Cell *41*, 180–194.e7.

Neutzner, A., Neutzner, M., Benischke, A.S., Ryu, S.W., Frank, S., Youle, R.J., and Karbowski, M. (2011). A systematic search for endoplasmic reticulum (ER) membrane-associated RING finger proteins identifies Nixin/ZNRF4 as a regulator of calnexin stability and ER homeostasis. J. Biol. Chem. *286*, 8633–8643.

Niu, L., Ma, T., Yang, F., Yan, B., Tang, X., Yin, H., Wu, Q., Huang, Y., Yao, Z.P., Wang, J., et al. (2019). Atlastin-mediated membrane tethering is critical for cargo mobility and exit from the endoplasmic reticulum. Proc. Natl. Acad. Sci. U S A *116*, 14029–14038.

Nucifora, F.C., Jr., Nucifora, L.G., Ng, C.H., Arbez, N., Guo, Y., Roby, E., Shani, V., Engelender, S., Wei, D., Wang, X.F., et al. (2016). Ubiquitination via K27 and K29 chains signals aggregation and neuronal protection of LRRK2 by WSB1. Nat. Commun. *7*, 11792.

O'Donnell, J.P., Cooley, R.B., Kelly, C.M., Miller, K., Andersen, O.S., Rusinova, R., and Sondermann, H. (2017). Timing and reset mechanism of GTP hydrolysis-driven conformational changes of atlastin. Structure *25*, 997–1010.e4.

Orso, G., Pendin, D., Liu, S., Tosetto, J., Moss, T.J., Faust, J.E., Micaroni, M., Egorova, A., Martinuzzi, A., McNew, J.A., et al. (2009). Homotypic fusion of ER membranes requires the dynamin-like GTPase atlastin. Nature *460*, 978–983.

Rismanchi, N., Soderblom, C., Stadler, J., Zhu, P.P., and Blackstone, C. (2008). Atlastin GTPases are required for Golgi apparatus and ER morphogenesis. Hum. Mol. Genet. *17*, 1591–1604.

Rolls, M.M., Hall, D.H., Victor, M., Stelzer, E.H., and Rapoport, T.A. (2002). Targeting of rough endoplasmic reticulum membrane proteins and ribosomes in invertebrate neurons. Mol. Biol. Cell *13*, 1778–1791.

Shibata, Y., Voeltz, G.K., and Rapoport, T.A. (2006). Rough sheets and smooth tubules. Cell *126*, 435–439.

Smith, M.H., Ploegh, H.L., and Weissman, J.S. (2011). Road to ruin: targeting proteins for degradation in the endoplasmic reticulum. Science *334*, 1086–1090.

Vembar, S.S., and Brodsky, J.L. (2008). One step at a time: endoplasmic reticulum-associated degradation. Nat. Rev. Mol. Cell Biol. *9*, 944–957.

Voeltz, G.K., Prinz, W.A., Shibata, Y., Rist, J.M., and Rapoport, T.A. (2006). A class of membrane proteins shaping the tubular endoplasmic reticulum. Cell *124*, 573–586.

Wang, S., Tukachinsky, H., Romano, F.B., and Rapoport, T.A. (2016). Cooperation of the ER-shaping proteins atlastin, lunapark, and reticulons to generate a tubular membrane network. Elife *5*, e18605.

Westrate, L.M., Lee, J.E., Prinz, W.A., and Voeltz, G.K. (2015). Form follows function: the importance of endoplasmic reticulum shape. Annu. Rev. Biochem. *84*, 791–811.

Zhang, T., Xu, Y., Liu, Y., and Ye, Y. (2015). gp78 functions downstream of Hrd1 to promote degradation of misfolded proteins of the endoplasmic reticulum. Mol. Biol. Cell *26*, 4438–4450.

Zhao, X., Alvarado, D., Rainier, S., Lemons, R., Hedera, P., Weber, C.H., Tukel, T., Apak, M., Heiman-Patterson, T., Ming, L., et al. (2001). Mutations in a newly identified GTPase gene cause autosomal dominant hereditary spastic paraplegia. Nat. Genet. *29*, 326–331.

Zhao, Y., Zhang, T., Huo, H., Ye, Y., and Liu, Y. (2016). Lunapark is a component of a ubiquitin ligase complex localized to the endoplasmic reticulum three-way junctions. J. Biol. Chem. *291*, 18252–18262.

Zhou, X., He, Y., Huang, X., Guo, Y., Li, D., and Hu, J. (2019). Reciprocal regulation between lunapark and atlastin facilitates ER three-way junction formation. Protein Cell *10*, 510–525.

iScience, Volume *23*

Supplemental Information

The E3 Ubiquitin Ligase SYVN1 Ubiquitinates Atlastins to Remodel the Endoplasmic Reticulum Network

Yupeng Zhao, Zhigang Feng, Yan Zou, and Yanfen Liu

Figure S1

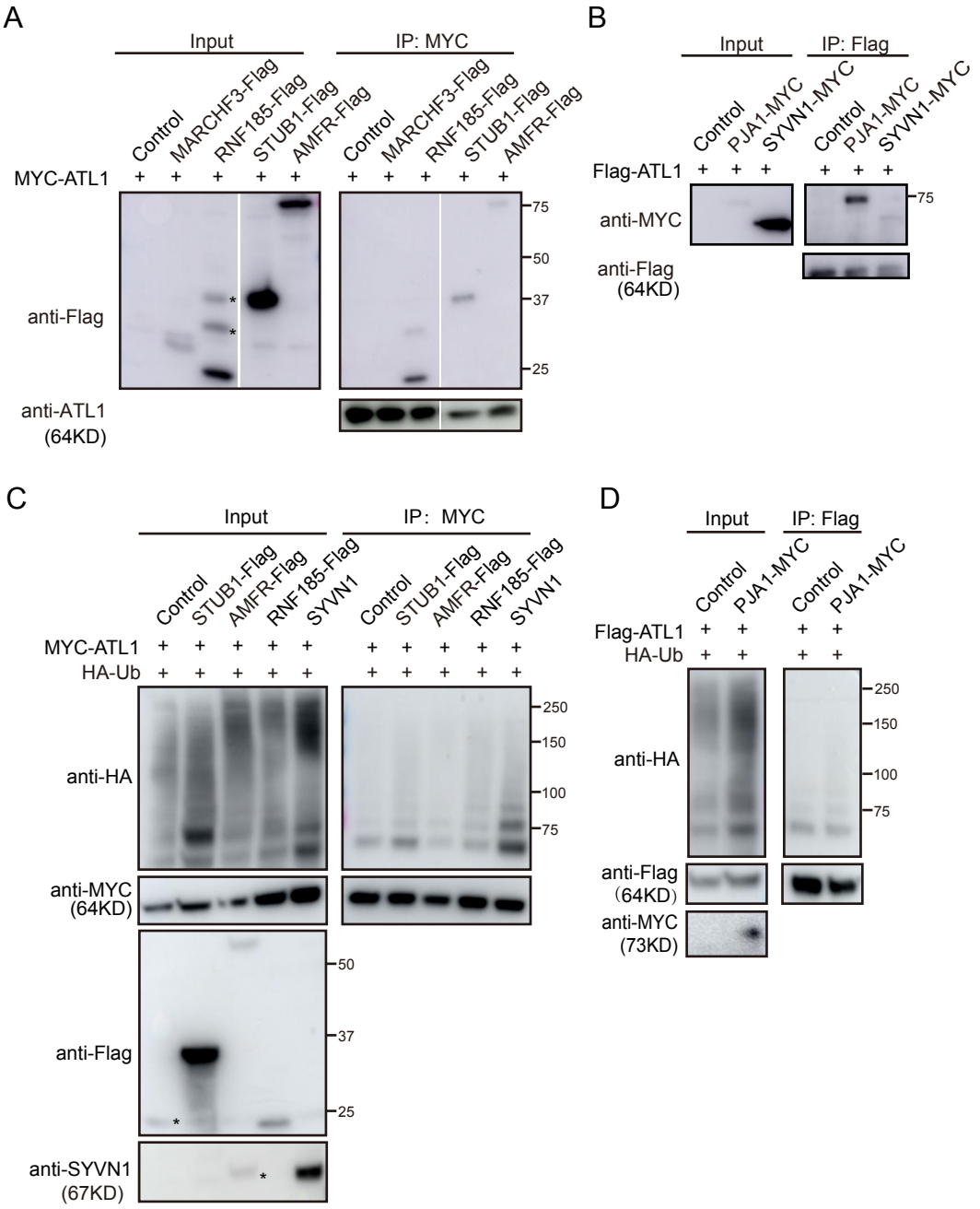
A
Input
IP: MYC
Control
MARCHF3-Flag
RNF185-Flag
STUB1-Flag
AMFR-Flag
MYC-ATL1
anti-Flag
anti-ATL1
(64KD)
75
50
37
25
B
Input
IP: Flag
Control
PJA1-MYC
SYVN1-MYC
Flag-ATL1
anti-MYC
anti-Flag
(64KD)
75
C
Input
IP: MYC
Control
STUB1-Flag
AMFR-Flag
RNF185-Flag
SYVN1
MYC-ATL1
HA-Ub
anti-HA
anti-MYC
(64KD)
anti-Flag
anti-SYVN1
(67KD)
250
150
100
75
50
37
25
D
Input
IP: Flag
Control
PJA1-MYC
Flag-ATL1
HA-Ub
anti-HA
anti-Flag
(64KD)
anti-MYC
(73KD)
250
150
100
75

Figure S2

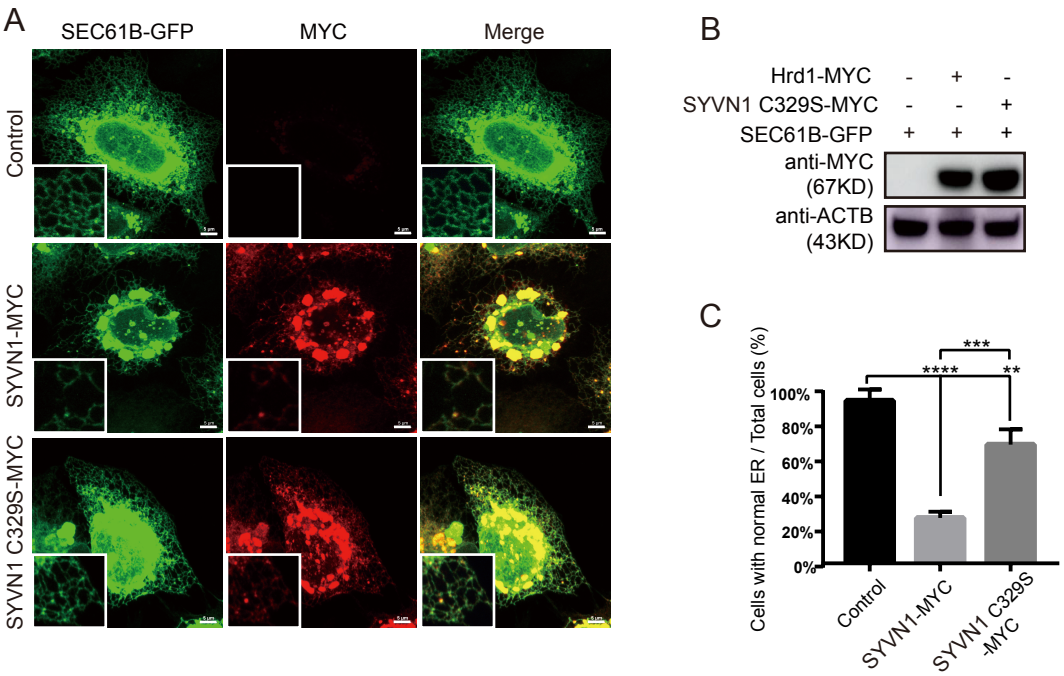
A
SEC61B-GFP
MYC
Merge
Control
SYVN1-MYC
SYVN1 C329S-MYC
B
Hrd1-MYC - + -
SYVN1 C329S-MYC - - +
SEC61B-GFP + + +
anti-MYC (67KD)
anti-ACTB (43KD)
C
Cells with normal ER / Total cells (%)
100%
80%
60%
40%
20%
0%
***
****
**
Control
SYVN1-MYC
SYVN1 C329S -MYC

Figure S3

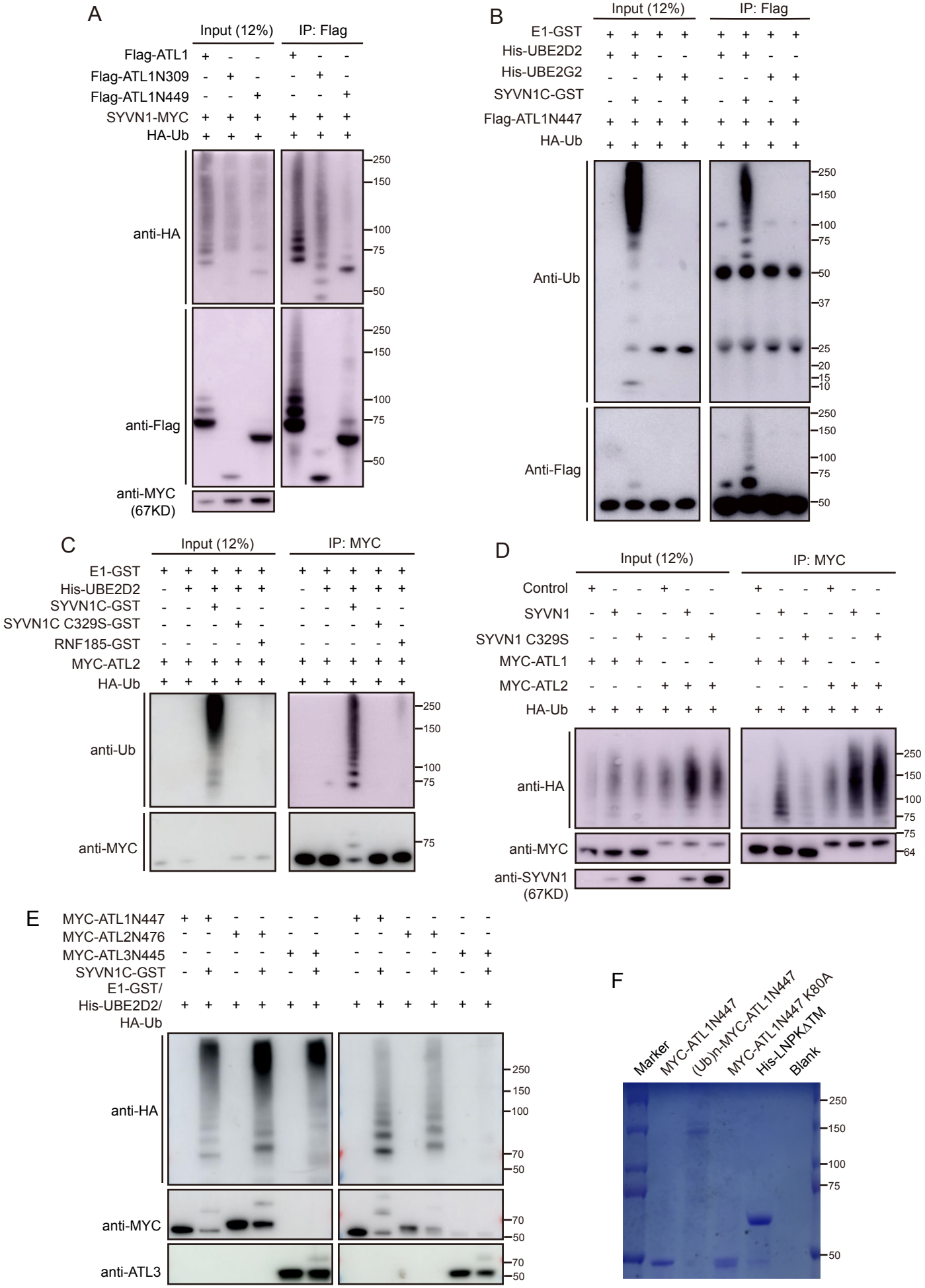
A
Input (12%)
IP: Flag
Flag-ATL1
Flag-ATL1N309
Flag-ATL1N449
SYVN1-MYC
HA-Ub
anti-HA
anti-Flag
anti-MYC (67KD)
B
Input (12%)
IP: Flag
E1-GST
His-UBE2D2
His-UBE2G2
SYVN1C-GST
Flag-ATL1N447
HA-Ub
Anti-Ub
Anti-Flag
C
Input (12%)
IP: MYC
E1-GST
His-UBE2D2
SYVN1C-GST
SYVN1C C329S-GST
RNF185-GST
MYC-ATL2
HA-Ub
anti-Ub
anti-MYC
D
Input (12%)
IP: MYC
Control
SYVN1
SYVN1 C329S
MYC-ATL1
MYC-ATL2
HA-Ub
anti-HA
anti-MYC
anti-SYVN1 (67KD)
E
MYC-ATL1N447
MYC-ATL2N476
MYC-ATL3N445
SYVN1C-GST
E1-GST/ His-UBE2D2/ HA-Ub
anti-HA
anti-MYC
anti-ATL3
F
Marker
MYC-ATL1N447
(Ub)n-MYC-ATL1N447
MYC-ATL1N447 K80A
His-LNPKΔTM
Blank

Figure S4

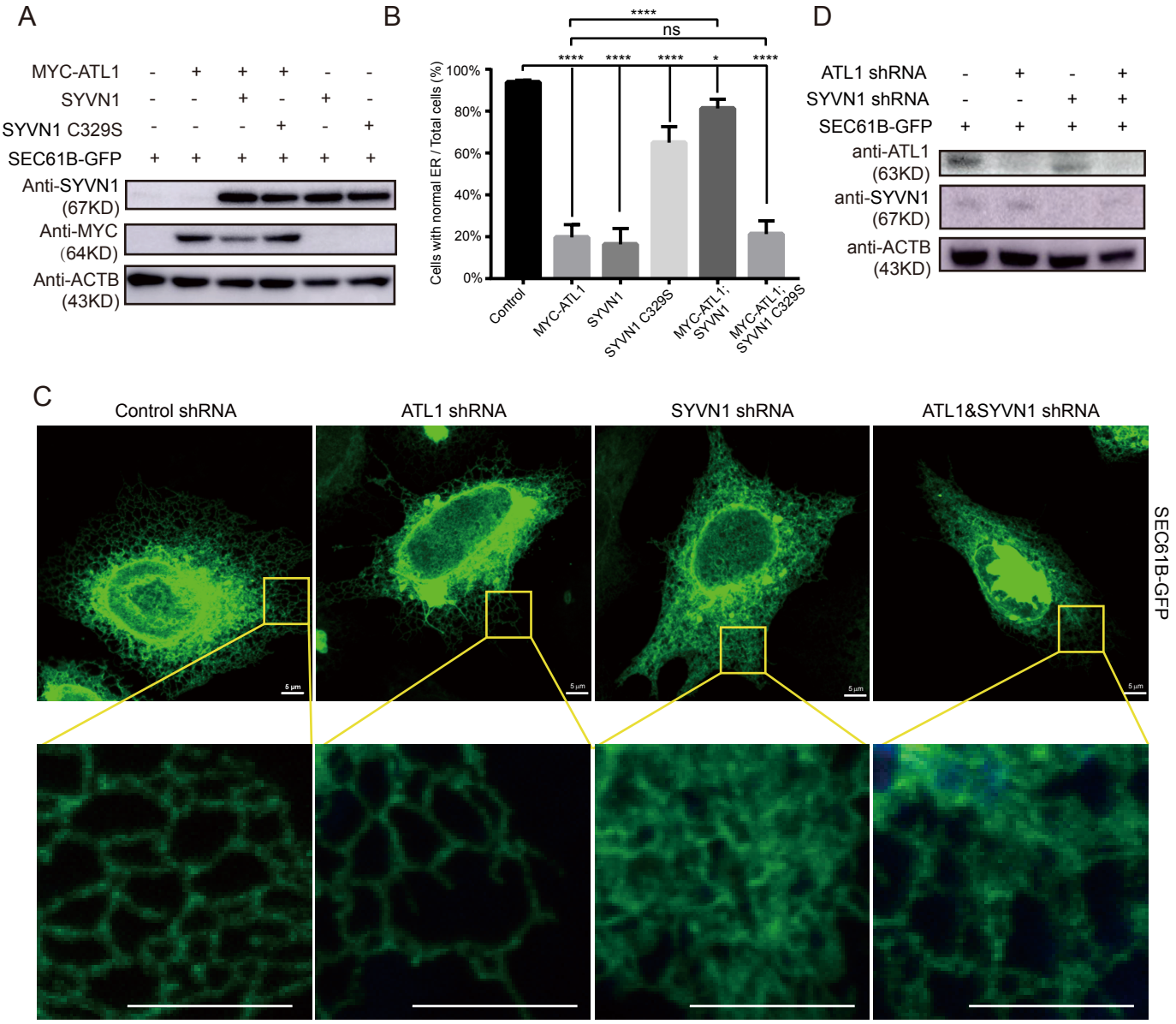
A
MYC-ATL1 - + + + - -
SYVN1 - - + - + -
SYVN1 C329S - - - + - +
SEC61B-GFP + + + + + +
Anti-SYVN1 (67KD)
Anti-MYC (64KD)
Anti-ACTB (43KD)
B
Cells with normal ER / Total cells (%)
100%
80%
60%
40%
20%
0%
****
ns
****
****
****
*
****
Control
MYC-ATL1
SYVN1
SYVN1 C329S
MYC-ATL1; SYVN1
MYC-ATL1; SYVN1 C329S
D
ATL1 shRNA - + - +
SYVN1 shRNA - - + +
SEC61B-GFP + + + +
anti-ATL1 (63KD)
anti-SYVN1 (67KD)
anti-ACTB (43KD)
C
Control shRNA
ATL1 shRNA
SYVN1 shRNA
ATL1&SYVN1 shRNA
SEC61B-GFP
5 μm

Figure S5

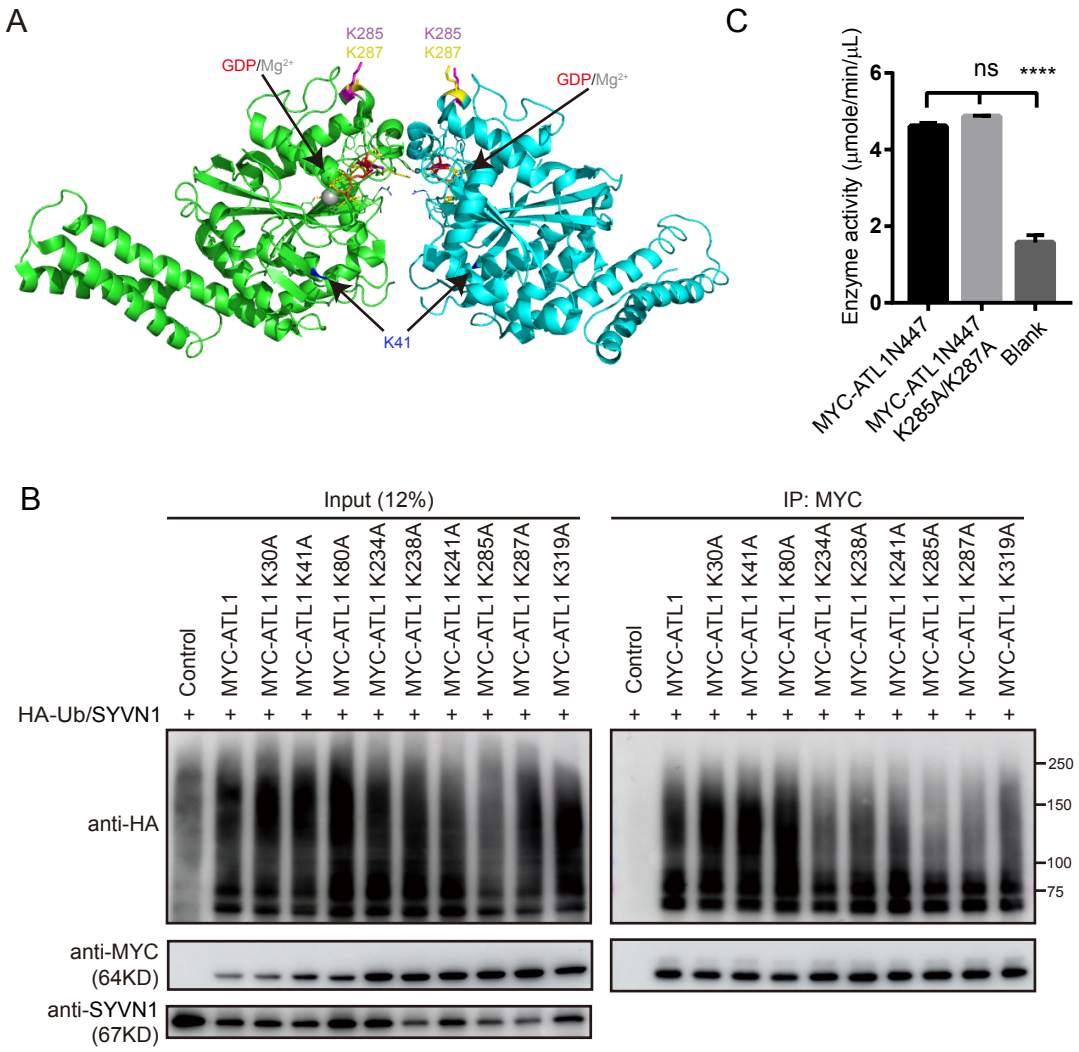
A
K285
K287
K285
K287
GDP/Mg2+
GDP/Mg2+
K41
C
Enzyme activity (μmole/min/μL)
ns
****
MYC-ATL1N447
MYC-ATL1N447 K285A/K287A
Blank
B
Input (12%)
IP: MYC
Control
MYC-ATL1
MYC-ATL1 K30A
MYC-ATL1 K41A
MYC-ATL1 K80A
MYC-ATL1 K234A
MYC-ATL1 K238A
MYC-ATL1 K241A
MYC-ATL1 K285A
MYC-ATL1 K287A
MYC-ATL1 K319A
HA-Ub/SYVN1
anti-HA
anti-MYC (64KD)
anti-SYVN1 (67KD)
250
150
100
75

Figure S6

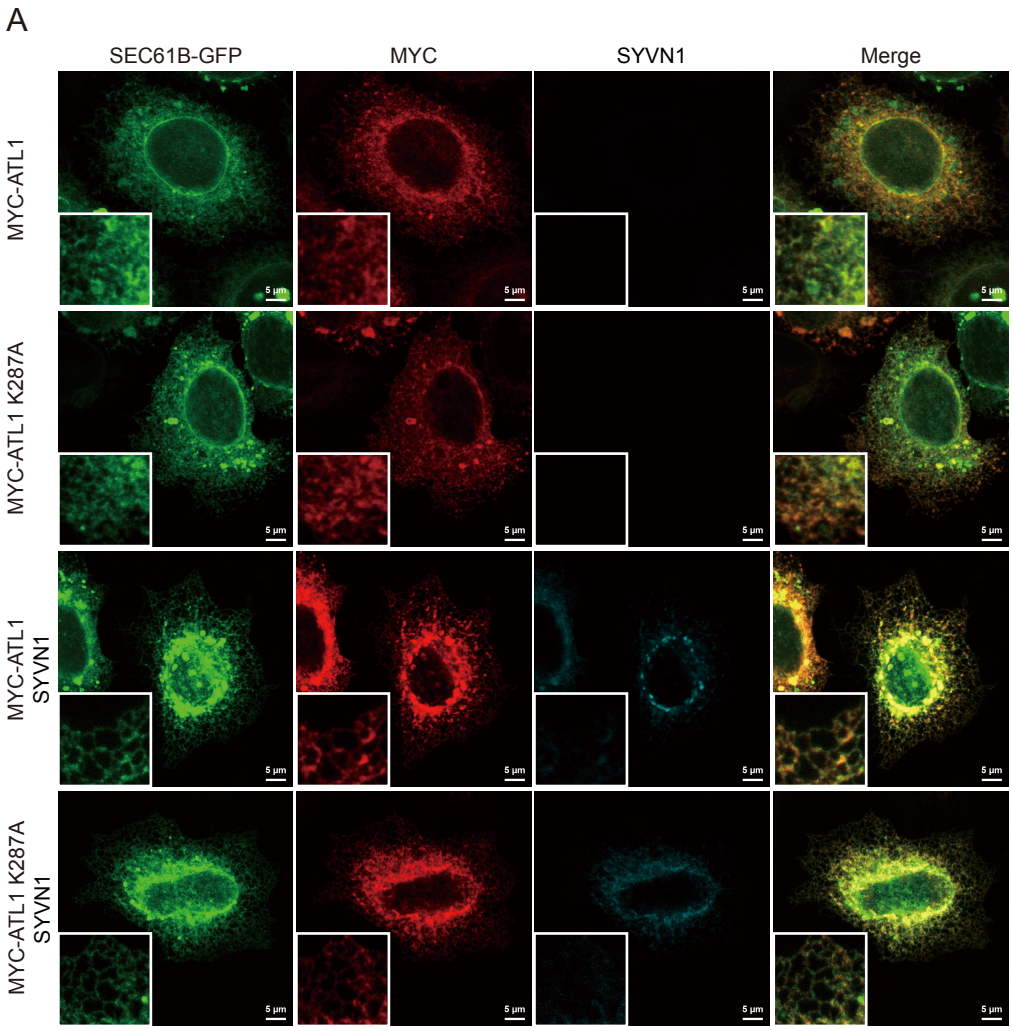
A
SEC61B-GFP
MYC
SYVN1
Merge
MYC-ATL1
MYC-ATL1 K287A
MYC-ATL1 SYVN1
MYC-ATL1 K287A SYVN1
5 μm

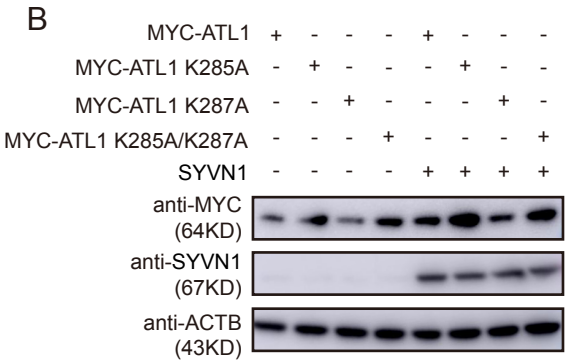
B
MYC-ATL1 + - - - + - - -
MYC-ATL1 K285A - + - - - + - -
MYC-ATL1 K287A - - + - - - + -
MYC-ATL1 K285A/K287A - - - + - - - +
SYVN1 - - - - + + + +
anti-MYC (64KD)
anti-SYVN1 (67KD)
anti-ACTB (43KD)

Figure S7

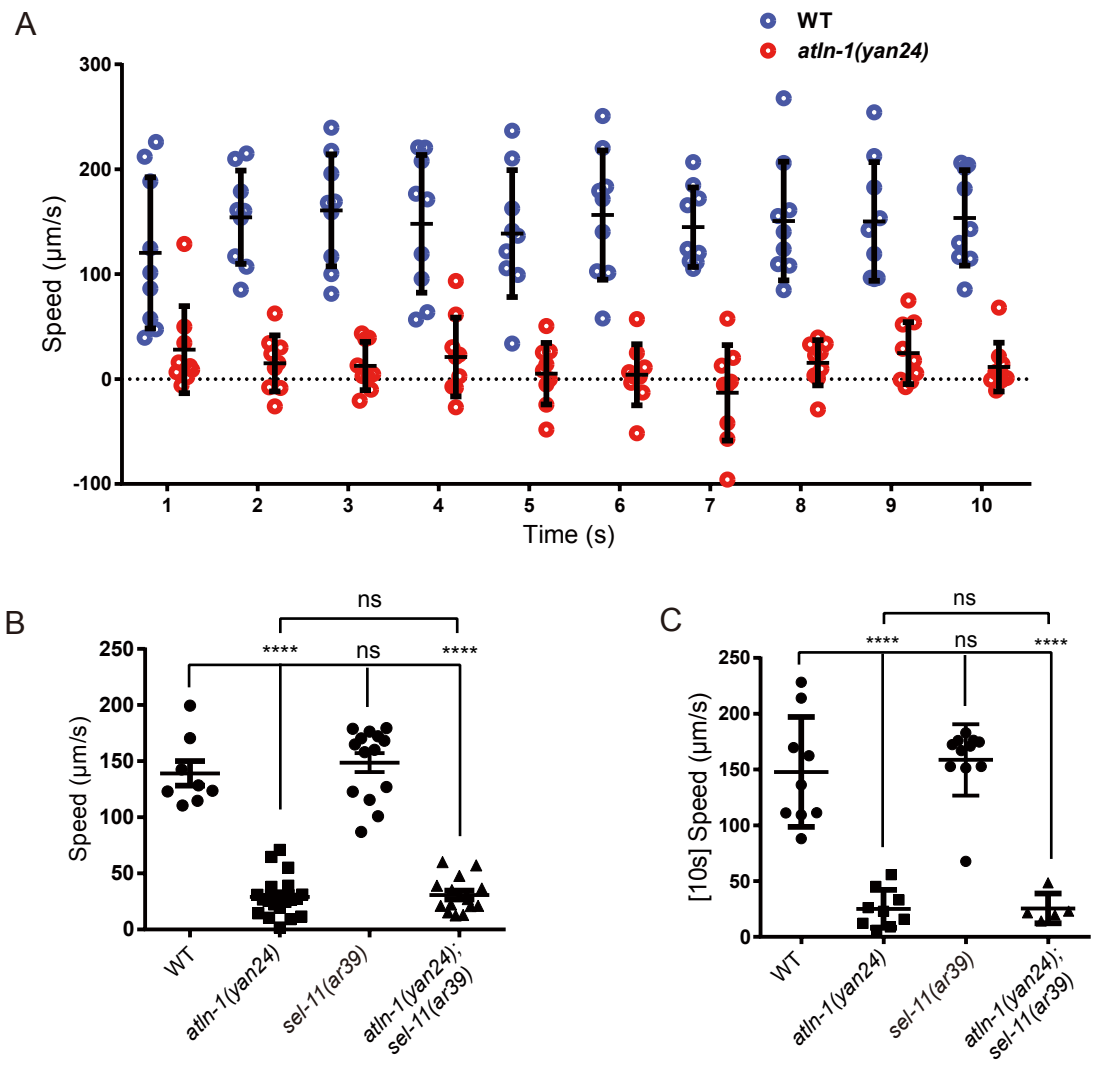
A
WT
atln-1(yan24)
Speed (µm/s)
300
200
100
0
-100
1
2
3
4
5
6
7
8
9
10
Time (s)
B
ns
****
ns
****
Speed (µm/s)
250
200
150
100
50
0
WT
atln-1(yan24)
sel-11(ar39)
atln-1(yan24); sel-11(ar39)
C
ns
****
ns
****
[10s] Speed (µm/s)
250
200
150
100
50
0
WT
atln-1(yan24)
sel-11(ar39)
atln-1(yan24); sel-11(ar39)

Supplemental Figure Legends

Figure S1. A screen for E3 ubiquitin ligases that interact with and ubiquitinate ATL1, Related to Figure 1.

(A and B) A screen for E3 ubiquitin ligases that interact with ATL1. HEK293FT cells were transfected with *MYC-ATL1*, along with Flag-tagged ER-localized E3 ubiquitin ligases *MARCHF3*, *RNF185*, *AMFR*, or the control cytosolic E3 ubiquitin ligase *STUB1* (A). HEK293FT cells were transfected with *Flag-ATL1*, along with MYC-tagged ER-localized E3 ubiquitin ligases *SYVN1* or the control cytosolic E3 ubiquitin ligase *PJA1* (B). After 24 h, anti-MYC immunoprecipitation (A) or Flag pulldown (B) was performed and the samples were analyzed by immunoblotting with the indicated antibodies.

(C and D) The ATL1-interacting E3 ubiquitin ligases were further tested for their ability to ubiquitinate ATL1. HEK293FT cells were transfected with *MYC-ATL1* and *HA-ubiquitin*, along with the control, the E3 ubiquitin ligase *STUB1-Flag*, *AMFR-Flag*, *RNF185-Flag*, or untagged *SYVN1* (C). HEK293FT cells were transfected with *Flag-ATL1* and *HA-ubiquitin*, along with the control or the E3 ubiquitin ligase *PJA1-MYC* (D). After 24 h, ubiquitinated ATL1 were immunoprecipitated with anti-MYC (C) or anti-Flag (D) beads under denaturing condition and immunoblotted with an anti-HA antibody.

Figure S2. The E3 ubiquitin ligase activity of SYVN1 contributes to ER shaping, Related to Figure 2.

(A) Representative images of HeLa cells transfected with the control, *SYVN1-MYC* or *SYVN1C329S-MYC*, together with the ER marker *SEC61B-GFP*. Cells were immunostained with the indicated antibodies. Scale bar, 5 μm.

(B) Immunoblotting analysis of the samples in (A).

(C) Statistical analysis of samples in (A) shows the ratio of cells with normal ER network. Data are represented as mean ± SD from three independent experiments. About 100 cells were counted in each group. **p < 0.01; ***p < 0.001; ****p < 0.0001 (one-sided ANOVA).

Figure S3. ATL1, ATL2 and only slight amount of ATL3, are ubiquitinated by SYVN1, Related to Figure 3.

(A) HEK293FT cells were transfected with *SYVN1-MYC* and *HA-ubiquitin*, along with *Flag-ATL1* or its truncation mutants. After 24 h, cells were immunoprecipitated under denaturing condition with anti-Flag beads. Samples were analyzed by immunoblotting.

(B) Bacterial purified Flag-ATL1N447 was incubated with E1-GST, His-UBE2D2 or His-UBE2G2, SYVN1C-GST and HA-ubiquitin at 37°C for 1 h for the ubiquitination assay. Samples were then immunoprecipitated under denaturing condition with anti-Flag beads. All samples were analyzed by immunoblotting.

(C) Mammalian purified MYC-ATL2 was incubated with E1-GST, His-UBE2D2, SYVN1C-GST or SYVN1C C329S-GST or RNF185-GST, and HA-ubiquitin at 37°C for 1 h for the ubiquitination assay. Immunoprecipitation under denaturing condition was performed with anti-MYC beads. Samples were analyzed by immunoblotting.

(D) *MYC-ATL1* or *MYC-ATL2*, *HA-ubiquitin* and *SYVN1* or *SYVN1C329S* were co-transfected into HEK293FT cells. After 24 h, immunoprecipitation under denaturing condition was performed with anti-MYC beads. Samples were analyzed by immunoblotting.

(E) Bacterial purified N-terminal cytosolic segments of ATLs were incubated with E1-GST, His-UBE2D2, SYVN1C-GST and HA-ubiquitin at 37°C for 1 h for the ubiquitinatation assay. Samples were then immunoprecipitated under denaturing condition with anti-MYC beads, and immunoblotted with anti-HA for ubiquitin and anti-MYC for ATL1 and ATL2. ATL3 was detected by an anti-ATL3 antibody.

(F) Coomassie staining result to show the protein amount used for the GTPase activity assay in Figure 2E.

Figure S4. SYVN1 and ATL1 cooperatively regulate ER dynamics, Related to Figure 4.

(A-B) Immunoblotting results and statistical analysis of the samples in Figure 4. Data are represented as mean ± SD from three experiments. About 100 cells were counted in each group. ns, not significant; ***$p < 0.001$; ****$p < 0.001$ (one-sided ANOVA).

(C) Representative images of HeLa cells transfected with the control shRNA, *ATL1* shRNA, or/and *SYVN1* shRNA, together with the ER marker *SEC61B-GFP*. 48 h after transfection, cells

were fixed and immunostained with the indicated antibodies. Scale bar, 5 μm.

(D) Immunoblotting analysis of the samples in (C).

Figure S5. An immunoprecipitation-based screen for the ubiquitination sites on ATL1 modified by SYVN1, Related to Figure 5.

(A) The spatial position of K285 and K287 in ATL1 dimer. GDP (red), Mg^{2+} (grey), K41 (dark blue), K285 (purple) and K287 (yellow) are highlighted in the structure of dimerized ATL1N446 bound to GDP/Mg^{2+}.

(B) SYVN1 ubiquitinates ATL1 on multiple sites. *SYVN1*, *HA-ubiquitin*, and *MYC-ATL1* or its lysine mutants were co-transfected into HEK293FT cells. After 24 h, cells were immunoprecipitated under denaturing condition with anti-MYC beads. Samples were analyzed by immunoblotting.

(C) Bacterial purified MYC-ATL1N447 and MYC-ATL1N447 K285A/K287A were tested for the GTPase activity assay. Data are represented as mean ± SD from three independent experiments. ns, not significant; ****$p < 0.0001$ (one-sided ANOVA).

Figure S6. K285 and K287 are the major ubiquitinated sites by SYVN1, Related to Figure 5.

(A) Representative images of HeLa cells transfected with *MYC-ATL1* or *MYC-ATL1 K287A*, along with the control or *SYVN1* (experiments done together with *ATL1K285A* and *ATL1K285A/K287A* mutants as shown in Figure 5B). After 24 h, cells were fixed and immunostained with the indicated antibodies. Scale bar, 5 μm.

(B) Immunoblotting analysis of the samples in Figure 5B and Figure S6A.

Figure S7. *atln-1* mutant has mobility defects, and *sel-11* mutant does not rescue this abnormality, Related to Figure 6.

(A) L4 stage worms of wild type strain and *atln-1(yan24)* mutant animals were selected for mobility test. Worms reaching young adult stage were cultured in separate plates for mobility recording. Nine worms were counted for each group.

(B) As in (A), wild-type, *atln-1(yan24)*, *sel-11(ar39)* and *atln-1(yan24)*;*sel-11(ar39)* were

analyzed to obtain the average speed during worms moved within the field of camera. Data are represented as mean ± SD. About 8~20 worms were counted in each group. ns, not significant; ****p < 0.0001 (one-sided ANOVA).

(C) As in (A), wild-type, *atln-1(yan24)*, *sel-11(ar39)* and *atln-1(yan24)*;*sel-11(ar39)* were analyzed to obtain the average speed of randomly selected 10 s. Data are represented as mean ± SD. Number of each group is 8~20. ns, not significant; ****p < 0.0001 (one-sided ANOVA).

Transparent Methods

Key Resources Table

REAGENT or RESOURCE	**SOURCE**	**IDENTIFIER**
Antibodies		
Rabbit polyclonal anti-Flag	Sigma-Aldrich	Cat#F7425
Mouse polyclonal anti-ACTB (HRP-DirecT)	Medical & Biological Laboratories Co., LTD.	Cat# PM053-7
Rabbit polyclonal anti-AMFR	(Li et al., 2009)	N/A
Rabbit monoclonal anti-HA	Cell Signaling Technology	Cat#3724
Mouse monoclonal anti-MYC	Cell Signaling Technology	Cat#2276
Mouse monoclonal anti-ubiquitin	Santa Cruz Biotechnology	Cat#sc-8017
Goat anti-mouse IgG (H+L), HRP	Jackson ImmunoResearch Inc.	Cat#111-035-146
Goat anti-rabbit IgG (H+L), HRP	Jackson ImmunoResearch Inc.	Cat#111-035-144
Goat anti-mouse IgG (H+L), Alexa Fluor 488	Thermo Fisher Scientific	Cat#A-11029
Goat anti-rabbit IgG (H+L), Alexa Fluor 568	Thermo Fisher Scientific	Cat#A-11036
Goat anti-rabbit IgG (H+L), Alexa Fluor 488	Thermo Fisher Scientific	Cat#A-11034
Goat anti-mouse IgG (H+L), Alexa Fluor 568	Thermo Fisher	Cat#A-11031

	Scientific	
Goat anti-rabbit IgG (H+L), Alexa Fluor 633	Thermo Fisher Scientific	Cat#A-21071
Rabbit polyclonal anti-ATL1	Proteintech	Cat#12149-1-AP
Rabbit polyclonal anti-ATL3	Abcam	Cat#ab117819
Rabbit monoclonal anti-SYVN1	Cell Signaling Technology	Cat#14773
Purified Mouse Anti-SEC31A	BD Biosciences	Cat#612350
Critical Commercial Assays		
ATPase/GTPase Activity Assay Kit	Sigma-Aldrich	Cat#MAK113
Anti-Flag beads	Bimake	Cat# B23102
Anti-MYC magnetic beads	Bimake	Cat# B26302
Bacterial Strains		
Trans5α Chemically Competent Cell	Transgen Biotech	Cat#CD201-01
BL21 Chemically Competent Cell	Transgen Biotech	Cat# CD901-01
Transetta (DE3) Chemically Competent Cell	Transgen Biotech	Cat# CD801-01
Chemicals		
Chloroquine	Sigma-Aldrich	Cat#C6628-25g
MG132	MedChemExpress	Cat#HY-13259
Protease inhibitor cocktail	Bimake	Cat#B14011
Experimental Models: Cell Lines		
HEK293FT	ATCC	N/A
HeLa	ATCC	N/A
Experimental Models: Strains		
C. elegans: BLW559 *ybqIs55[flp-13p::tagRFP::tram-1]*; *Ex[flp-13p::GFP]*	Yingchuan Qi (Shanghaitech University)	N/A
C. elegans: ZOU500	This paper	N/A

sel-11(ar39); *ybqIs55*; *Ex[flp-13p::GFP]*		
C. elegans: ZOU501 *atln-1(yan24)*/tmC25[*unc-5(tmIs1241)*]; *ybqIs55*; *Ex[flp-13p::GFP]* *yan24:* aatttcagaaaaagtgccaa--(deletion sizes 691bp)--GGGAGgtataatatatttta	This paper	N/A
C. elegans: ZOU502 *atln-1(yan24)*/tmC25*[unc-5(tmIs1241)]*; *sel-11(ar39)*; *ybqIs55*; *Ex[flp-13p::GFP]*	This paper	N/A
C. elegans: ZOU503 *ybqIs55*; *yanEx316[rgef-1p::atln-1 + flp-13p::GFP]*	This paper	N/A
C. elegans: ZOU504 *ybqIs55*; *yanEx317[rgef-1p::sel-11 + flp-13p::GFP]*	This paper	N/A
C. elegans: ZOU505 *ybqIs55*; *yanEx318[rgef-1p::sel-11(C295Y) + flp-13p::GFP]*	This paper	N/A
C. elegans: ZOU506 *ybqIs55*; *yanEx316[rgef-1p::atln-1 + flp-13p::GFP]*; *yanEx317[rgef-1p::sel-11 + flp-13p::GFP]*	This paper	N/A
C. elegans: ZOU507 *ybqIs55*; *yanEx316[rgef-1p::atln-1 + flp-13p::GFP]*; *yanEx318[rgef-1p::sel-11(C295Y) + flp-13p::GFP]*	This paper	N/A
Oligonucleotides		
Human *ATL1* shRNA targeting sequence: CCATTCCTGTTTCACCAACAT	This paper	N/A

Human *SYVN1* shRNA targeting sequence: GCAAGGTGATGGGCAAGGTGT	This paper	N/A
C. elegans atln-1 sgRNA site-1: TGCTTGAATTATCCAGAGA	This paper	N/A
C. elegans atln-1 sgRNA site-2: ATGGAGATCGAAAGCTGATA	This paper	N/A
Recombinant DNA		
pGW1-MYC-ATL1	(Hu et al., 2009)	N/A
pGW1-MYC-ATL2	(Hu et al., 2009)	N/A
pGW1-MYC-ATL3	(Hu et al., 2009)	N/A
pCMV-SYVN1	Yihong Ye (National Institutes of Health, USA)	N/A
pCMV-SYVN1C329S	This paper	N/A
pcDNA3.1-SYVN1-MYC/His A(-)	(Liu et al., 2014)	N/A
pcDNA3-Flag-MARCHF3	This paper	N/A
pcDNA3-Flag-RNF185	This paper	N/A
pRK5-Flag-STUB1	(Chu et al., 2020)	N/A
pCMV6-PJA1-MYC	This paper	N/A
pcDNA3-AMFR-Flag	(Zhao et al., 2016)	N/A
AMFR shRNA	Shenyun Fang (University of Maryland)	N/A
pCDNA3.1-SEC61B-GFP	(Shibata et al., 2008)	N/A
E1-GST	Wei Li (Chinese Academy of Sciences)	N/A

pETSUMO-His-SUMO-UBE2D2	(Wiener et al., 2013)	N/A
pET32a(+)-His-TEV-UBE2D2	This paper	N/A
pET32a(+)-His-TEV-UBE2G2	This paper	N/A
pGEX-6p-1-SYVN1C-GST	This paper	N/A
pGEX-6p-1-SYVN1C C329S-GST	This paper	N/A
pGEX-6p-1-RNF185-GST	This paper	N/A
pRK5-HA-ubiquitin	(Liu et al., 2014)	N/A
pT7-7-His-Flag-ubiquitin	Kazuhiro Iwai (Kyoto University)	N/A
pT7-7-His-HA-ubiquitin	Kazuhiro Iwai (Kyoto University)	N/A
pRK5-Flag-ATL1	This paper	N/A
pRK5-Flag-ATL1N449 (1-449aa)	This paper	N/A
pRK5-Flag-ATL1N309 (1-309aa)	This paper	N/A
pRK5-Flag-ATL1C310 (310-558aa)	This paper	N/A
pRK5-Flag-ATL1C450 (450-558aa)	This paper	N/A
pGW1-MYC-ATL1K30A	This paper	N/A
pGW1-MYC-ATL1K41A	This paper	N/A
pGW1-MYC-ATL1K80A	This paper	N/A
pGW1-MYC-ATL1K234A	This paper	N/A
pGW1-MYC-ATL1K238A	This paper	N/A
pGW1-MYC-ATL1K241A	This paper	N/A
pGW1-MYC-ATL1K285A	This paper	N/A
pGW1-MYC-ATL1K287A	This paper	N/A
pGW1-MYC-ATL1K319A	This paper	N/A
pET32a(+)-His-TEV-Flag-ATL1N447	This paper	N/A
pET32a(+)-His-TEV-MYC-ATL1N447	This paper	N/A
pET32a(+)-His-TEV-MYC-ATL1N447 K80A	This paper	N/A

pET32a(+)-His-TEV-MYC-ATL1N447 K285A	This paper	N/A
pET32a(+)-His-TEV-MYC-ATL1N447 K287A	This paper	N/A
pET32a(+)-His-TEV-MYC-ATL1N447 K285A/K287A	This paper	N/A
pET32a(+)-His-TEV-MYC-ATL2N476	This paper	N/A
pET32a(+)-His-TEV-MYC-ATL3N445	This paper	N/A
pET32a(+)-His-TEV-LNPKΔTM	(Zhao et al., 2016)	N/A
pSUPER.neo	OligoEngine	Cat# VEC-PBS-0004
pSM-rgef-1p::atln-1	This paper	N/A
pSM-rgef-1p::sel-11	This paper	N/A
pSM-rgef-1p::sel-11C295Y	This paper	N/A
pQ615-Flp-13p::GFP	Yingchuan Qi (Shanghaitech University)	N/A
Software and Algorithms		
Prism 7	GraphPad	https://www.graphpad.com/scientific-software/prism/
ImageJ	NIH	https://imagej.nih.gov/ij/
Wormlab	MBF Bioscience	https://www.wordlab.com/

Cell lines

HEK293FT cell line and HeLa cell line were obtained from ATCC and were cultured in DMEM (Gibco) with 10% fetal bovine serum (Gemini) and 100 U/ml penicillin G and 100 μg/ml streptomycin (Thermo Fisher Scientific) at 37°C under 5% CO_2.

C. elegans

C. elegans animals were grown on OP50 *E. coli*-seeded nematode growth medium (NGM) plates at 20°C following standard protocols (Brenner, 1974). Transgenic strains were generated with the microinjection of 50 ng/μl recombinant DNA into BLW559 germlines. Conditional knockout *C. elegans* were generated using the CRISPR/Cas9 strategy and verified by PCR and sequence analysis.

Plasmids

Mammalian expression constructs for *pcDNA3.1-SYVN1-MYC/His A(-)* and *pRK5-HA-ubiquitin* were described previously (Liu et al., 2014). Constructs for expressing *pET32a(+)-His-TEV-LNPKΔTM* and *pcDNA3-AMFR-Flag* were described previously (Zhao et al., 2016). Constructs for expressing *pRK5-Flag-STUB1* was described previously (Chu et al., 2020). *pGW1-MYC-ATL1*, *pGW1-MYC-ATL2* and *pGW1-MYC-ATL3* were kindly provided by Dr. Junjie Hu (Chinese Academy of Sciences). Construct for expressing *E1-GST* was kindly gifted by Dr. Wei Li (Chinese Academy of Science). The construct for expression of *pETSUMO-His-SUMO-UBE2D2* was kindly provided by Dr. Cynthia Wolberger (John Hopkins University) (Wiener et al., 2013). *pCMV-SYVN1* and *pCDNA3.1-SEC61B-GFP* were provided by Dr. Yihong Ye (National Institutes of Health, USA). The constructs *pT7-7-His-Flag-ubiquitin* and *pT7-7-His-HA-ubiquitin* for expressing the recombinant ubiquitin were kindly provided by Professor Kazuhiro Iwai (Kyoto University). *pcDNA3-Flag-MARCHF3* and *pcDNA3-Flag-RNF185* were generated by inserting *MARCHF3* or *RNF185* fragment into *pcDNA3-Flag* vector. *pCMV6-PJA1-MYC* was generated by inserting *PJA1* into *pCMV6-MYC* vector. *SYVN1C329S* mutants were generated based on PCR-mediated site-directed mutagenesis on *pCMV-SYVN1* construct. *MYC-ATL1 K30A*, *MYC-ATL1 K41A*, *MYC-ATL1 K80A*, *MYC-ATL1 K234A*, *MYC-ATL1 K238A*, *MYC-ATL1 K241A*, *MYC-ATL1 K285A*, *MYC-ATL1 K287A* and *MYC-ATL1 K319A* were generated based on PCR-mediated site-directed mutagenesis on *pGW1-MYC-ATL1*. All mutations were confirmed by DNA sequencing. For expressing the recombinant proteins, *His-TEV-UBE2D2*, *His-TEV-UBE2G2*, *His-TEV-Flag-ATL1N447*, *His-TEV-MYC-ATL1N447*, *His-TEV-MYC-ATL1N447 K80A*, *His-TEV-MYC-ATL1N447 K285A*, *His-TEV-MYC-ATL1N447 K287A*, *His-TEV-MYC-ATL1N447 K285A/K287A*, *His-TEV-MYC-ATL2N476*, and *His-TEV-MYC-ATL3N445* fragments were constructed into *pET32a(+)*. *SYVN1C-GST* and

RNF185-GST were constructed into *pGEX-6p-1*. Plasmids for overexpressing in *C. elegans* (*rgef-1::atln-1*, *rgef-1::sel-11*, *rgef-1::sel-11C295Y*) were generated by inserting the fragments into *pSM* vector. The *pSUPER.neo* was used as the knockdown control and the backbone to generate the shRNA knockdown plasmids of *ATL1* and *SYVN1*. *ATL1* shRNA targeting sequence: 5'-CCATTCCTGTTTCACCAACAT; *SYVN1* shRNA site: 5'-GCAAGGTGATGGGCAAGGTGT. *AMFR* shRNA and control were provided by Dr. Shenyun Fang (University of Maryland).

Protein expression and purification

Mammalian expressed MYC-ATL1 was purified from HEK 293FT cells by the MYC magnetic beads (Bimake) following the standard immunoprecipitation procedure. GST- or His-tagged proteins expressed in bacteria were eluted from Glutathione-Sepharose beads (GE Healthcare) or Ni Sepharose (GE Healthcare), and then fractionated on a Superdex 200 HR (10/30) column (GE Healthcare) in the buffer containing 50 mM Tris-HCl (pH 8.0), 150 mM potassium chloride, 2 mM magnesium chloride, 2 mM DTT. To remove His tag from some proteins, TEV protease was applied for 48 h at 4°C followed by going through the Ni Sepharose to eliminate the unwanted proteins.

To purify untagged ubiquitin, bacteria expressing ubiquitin were first lysed with 20mM Na-Acetate (pH 5.1). After centrifuge, the supernatant was heated at 60°C for 20 min. The sample was then filtered and loaded onto a HiTrap SP HP column (GE Healthcare). Eluted with 20 mM sodium acetate (pH 5.1)/0-500 mM sodium chloride gradient, the fraction with ubiquitin was then buffer-changed to 20 mM Tris-HCl (pH 7.5) through a HiTrap DEAE FF column (GE Healthcare).

Immunoprecipitations and immunoblotting

Plasmids were transfected into HEK293FT cells and cell lysates were extracted by NP40 lysis buffer (50 mM Tris–HCl pH 7.4, 150 mM sodium chloride, and 0.5% NP40) containing 1% protease inhibitor cocktail (Bimake). For immunoprecipitation, the whole cell extract was incubated with Flag beads (Bimake) or MYC magnetic beads (Bimake) or protein A-Sepharose CL-4B (GE Healthcare) bound with antibodies against target proteins. After binding, the beads

were washed three times with NP40 wash buffer (50 mM Tris–HCl pH 7.4, 150 mM sodium chloride, and 0.1% NP40) to remove nonspecific binding proteins. The beads-bound material was eluted using Laemmli buffer and analyzed by immunoblotting. For immunoprecipitation under denaturing conditions, harvested cells were lysed in a buffer with 1% SDS and 5 mM DTT. The samples were heated at 65°C for 5 min and diluted into 0.1% SDS and 0.5 mM DTT with lysis buffer. The soluble supernatant fractions were harvested and subjected to immunoprecipitation experiments as described above. After that, immunoblotting was performed.

Immunofluorescence microscopy

HeLa cells were seeded at $1.75X10^5$/well in 6 well plates with small glass slides (10mm diameter), and were transiently transfected with the desirable plasmids. After 24 h or 48 h, the slides were fixed with PBS containing 4% paraformaldehyde and 4% sucrose for 15 min at room temperature. Subsequently, fixed cells were incubated in PBS containing 0.1% NP40 and 4% fetal bovine serum, and stained with antibodies in the same buffer according to the standard protocol. Images were acquired using a Zeiss LSM710 confocal microscope, with a 60 × 1.12 NA oil objective, with optical sections acquired 0.2 μm apart in the *z* axis.

***In vitro* ubiquitination assay**

Substrate (~3.6 μM) was incubated with E1-GST (704 nM), E2 (5.8 μM), E3 (5.7 μM) and ubiquitin (13.1 μM) in the reaction buffer containing 25 mM Tris-HCl pH 7.4, 2 mM magnesium/ATP and 1 mM DTT at 37°C for 1 h. After the reaction finished, the product was then immunoprecipitated with Flag or MYC beads under denaturing condition and the samples were analyzed by western blot.

GTPase activity assay

His-TEV-MYC-ATL1N447 was purified from bacteria and cleaved by TEV. The purified MYC-ATL1 was then applied for the ubiquitination assay by incubating with E1-GST, UBE2D2 (untagged), SYVN1C-GST and His-HA-ubiquitin. After ubiquitination reaction, $(His\text{-}HA\text{-}Ub)_n$-MYC-ATL1 was passed through the Ni Sepharose and then eluted by Buffer R (20 mM Tris-

HCl pH 8.0, 500 mM potassium chloride, glycerol 10%) with 250 mM imidazole. The sample was then buffer-exchanged to the storage buffer (100mM Tris-HCl pH 8.0, 50 mM sodium chloride, 2mM 2-Mercaptoethanol), and the excessive free ubiquitin was also removed. Same moles of $(His\text{-}HA\text{-}Ub)_n$-MYC-ATL1N447 and MYC-ATL1N447 were taken for the GTPase activity assay (Sigma-Aldrich). The proteins were incubated with GTPase activity assay buffer (20 µl) and GTP (4 mM, 10 µl) for 60 min at 25°C. After that, 200 µl reagent buffer was added to each sample for termination. After incubation for 30 min, the samples were measured at wavelength of 620 nm in a Plate Reader (PerkinElmer). A standard curve was also made for calculating the amount of phosphate. The GTPase activity was calculated as follows:

$$\text{Enzyme activity (µmole/min/µL)} = \frac{\text{Amount of phosphate released X Reaction volume}}{\text{Reaction time X Sample volume}}$$

Each sample has three parallel repeats. And the whole experiment was repeated twice. The six times measuring results was then analyzed to get an average and deviation.

C. elegans fluorescent imaging

Fluorescent imaging was performed as described before (Liu and Shen, 2011). L4 larval worms were anesthetized with 5 mM levamisole and mounted on 2% agarose pads at 20°C. The immobilized larvae were subsequently imaged with Nikon A1 R confocal microscope equipped with a 40 ×, N.A. 1.30, W.D. 0.2 mm DIC N2 objective, and the 568 nm lines Laser System. Z stacks (0.35 µm/step) and maximum-intensity projections were generated using ImageJ (NIH). ImageJ was used to generate complete pictures containing all five motor neurons of worms, and to generate straightened axons to count the distribution of TRAM-1.

Locomotion behavior analysis

Locomotion behavior analysis of *C. elegans* was performed as described (Lim et al., 2016). Briefly, young adult worms were transferred to 35 mm NGM plates thinly seeded with OP50 bacteria to perform automated tracking and behavioral analyses. Prior to recording, worms were placed in the center of the plates separately and allowed to habituate for 5 min. Behavior was recorded by Olympus MVX10 microscope equipped with BioHD-C20 camera, and the time worms moved in field of view was recorded. Using Wormlab (MBF Bioscience), we analyzed

and quantified the momentary speed and average speed of animals move forward and backward.

Statistical analysis

For the cell-based analysis, data were shown as mean ± SD, and error bars represented the standard deviations from counting of at least 100 cells in each group from three independent experiments. For the worm experiments, at least 8 samples from each group were collected for the statistical analysis. All statistical analyses were treated with GraphPad Prism version 7.0, and were performed with one-sided ANOVA with the Tukey correction (to test for differences between three or more groups). Statistical significance is represented in figures by *$p < 0.05$; **$p < 0.01$; ***$p < 0.001$; ****$p < 0.0001$; and ns for not significant.

Supplemental References

Brenner, S. (1974). The genetics of Caenorhabditis elegans. Genetics *77*, 71-94.

Chu, Y., Kang, Y., Yan, C., Yang, C., Zhang, T., Huo, H., and Liu, Y. (2020). LUBAC and OTULIN regulate autophagy initiation and maturation by mediating the linear ubiquitination and the stabilization of ATG13. Autophagy, 1-16.

Hu, J., Shibata, Y., Zhu, P.P., Voss, C., Rismanchi, N., Prinz, W.A., Rapoport, T.A., and Blackstone, C. (2009). A class of dynamin-like GTPases involved in the generation of the tubular ER network. Cell *138*, 549-561.

Li, W., Tu, D., Li, L., Wollert, T., Ghirlando, R., Brunger, A.T., and Ye, Y. (2009). Mechanistic insights into active site-associated polyubiquitination by the ubiquitin-conjugating enzyme Ube2g2. Proc. Natl. Acad. Sci. U S A. *106*, 3722-3727.

Lim, M.A., Chitturi, J., Laskova, V., Meng, J., Findeis, D., Wiekenberg, A., Mulcahy, B., Luo, L., Li, Y., Lu, Y.*, et al.* (2016). Neuroendocrine modulation sustains the C. elegans forward motor state. Elife *5*.

Liu, O.W., and Shen, K. (2011). The transmembrane LRR protein DMA-1 promotes dendrite branching and growth in C. elegans. Nat. Neurosci. *15*, 57-63.

Liu, Y., Soetandyo, N., Lee, J.G., Liu, L., Xu, Y., Clemons, W.M., Jr., and Ye, Y. (2014). USP13 antagonizes gp78 to maintain functionality of a chaperone in ER-associated degradation. Elife *3*, e01369.

Shibata, Y., Voss, C., Rist, J.M., Hu, J., Rapoport, T.A., Prinz, W.A., and Voeltz, G.K. (2008). The reticulon and DP1/Yop1p proteins form immobile oligomers in the tubular endoplasmic reticulum. J. Biol. Chem. *283*, 18892-18904.

Wiener, R., DiBello, A.T., Lombardi, P.M., Guzzo, C.M., Zhang, X., Matunis, M.J., and Wolberger, C. (2013). E2 ubiquitin-conjugating enzymes regulate the deubiquitinating activity of OTUB1. Nat. Struct. Mol. Biol. *20*, 1033-1039.

Zhao, Y., Zhang, T., Huo, H., Ye, Y., and Liu, Y. (2016). Lunapark Is a Component of a Ubiquitin Ligase Complex Localized to the Endoplasmic Reticulum Three-way Junctions. J. Biol. Chem. *291*, 18252-18262.